Final Draft
of the original manuscript:

Zeng, R.; Lan, Z.; Kong, L.; Huang, Y.; Cui, H.:
Characterization of calcium-modified zinc phosphate conversion coatings and their influences on corrosion resistance of AZ31 alloy
In: Surface & Coatings Technology (2010) Elsevier

DOI: 10.1016/j.surfcoat.2010.11.027

Characterization of calcium-modified zinc phosphate conversion coatings and their influences on corrosion resistance of AZ31 alloy

Rongchang Zeng [a, b *], Zidong Lan [b], Linghong Kong[a], Yuanding Huang[c], Hongzhi Cui [a]

[a] School of Materials Sciences and Engineering, Shandong University of Science and Technology, Qingdao 266510, China

[b] School of Materials Sciences and Engineering, Chongqing University of Technology, Chongqing 400050, China

[c] MagIC—Magnesium Innovation Center, GKSS Forschungszentrum Geesthacht GmbH, Geesthacht D-21502, Germany

[*] **Corresponding author**: School of Materials Sciences and Engineering, Shandong University of Science and Technology, Qingdao 266510, China.
Tel: +86-532-86081226.
E-mail: rczeng2001@yahoo.com.cn (R.C. Zeng)

Abstract: Two kinds of phosphate conversion coatings, including zinc phosphate coating and zinc-calcium phosphate coating, were prepared on the surface of AZ31 alloy in phosphate baths. The morphologies of these coatings were observed using scanning electron microscopy. Their chemical compositions and structures were characterized using energy-dispersive X-ray spectrum, X-ray photoelectron spectroscopy and X-ray diffraction. The corrosion resistance of the coatings was evaluated by potentiodynamic electrochemical technique. The results show that the flowerlike Zn-Ca phosphate conversion coatings mainly compose of hopeite ($Zn_3(PO_4)_2 \cdot 4H_2O$). They have a quite different morphology from the dry-riverbed-like Zn phosphate coatings that consist of MgO, MgF_2, Zn or ZnO and hopeite. Both of the zinc and zinc-calcium phosphate coatings can remarkably reduce the corrosion current density of the substrates. The Zn-Ca coating exhibits better corrosion resistance than the Zn coating. Introduction of calcium into the phosphate baths leads to the full crystallinity of the Zn-Ca coating.

Key words: phosphate conversion coating; magnesium alloy; corrosion; calcium; zinc

1 Introduction

Magnesium alloys are the lightest metals developed for structural applications such as aerospace and automobile industries [1]. Their applications are currently still not as popular as aluminum alloys because of their poor corrosion resistance [1-2]. To improve their corrosion resistance, one of the most effective approaches is to prepare a coating that can protect the substrates by providing a non-reactive barrier between the metal and its environment. These so-called surface modifications include anodic oxidation [3], electro-less plating [4] and chemical conversion coating [5-11]. Among these approaches, the chemical conversion coatings such as chromate conversion coating [5] has been widely used due to their lower cost and easier operation. However, one of the major components (Cr^{6+}) is detrimental to the environment. It is therefore necessary to find a substitute process with Cr^{6+}-free. The phosphate conversion coatings demonstrate a promising application and were considered to be environmentally friendly [12, 13].

The phosphate coatings on steels are categorized into five kinds [13]: zinc system coating [19], zinc calcium system, manganese system [20], manganese iron system and iron system coating [21]. However, not all of these coatings are suitable for magnesium alloys. Till now, zinc [18], stannate and manganese [14, 22-23] as well as molybdate/phosphate composite conversion coating [24] were reported to be suitable for magnesium alloys. Niu [18] investigated the zinc phosphate coating on AZ91D alloy. They found that the obtained coat has a typical phosphate microstructure, and consists of $Zn_3(PO_4)_2$ $4H_2O$, Zn, $AlPO_4$ and $MgZn_2(PO_4)_2$. However, Kouisni [16], Li [25] and Zeng [26] suggested that a well-crystallized zinc phosphate layer, which was formed in phosphating solutions, predominantly consists of hopeite ($Zn_3(PO_4)\cdot 4H_2O$). Han et al. [27] obtained a phosphate film

with $Mn_3(PO_4)_2$ on AZ31D alloy in a bath containing phosphate and manganese. All these coatings can more or less improve the corrosion resistance of magnesium alloys.

Introduction of calcium into the phosphate conversion baths results in a microstructural refinement of coatings and consequently an improvement of corrosion resistance [15]. It was reported that the introduction of calcium ions into a Mn-containing phosphate bath can modify the quality of the phosphate conversion coatings on magnesium alloys [23]. A Zn-Ca phosphate conversion coating with homogenous fine grains on the surface of magnesium alloy AZ31 was successfully prepared, which exhibits very good corrosion resistance [26]. However, the beneficial effects of the introduction of calcium on the coatings are not yet well understood. More investigations on this novel zinc-calcium phosphate coating are needed. Therefore, the present work explores the influence of the introduced calcium on the zinc phosphate conversion coatongs through a comparison between zinc phosphate coating and Zn-Ca coating.

2 Experimental

The materials used were an extruded AZ31 sheet (nominal chemical composition: 3 wt. % Al, 1 wt. % Zn and Mg, Bal.). The plates were machined into samples with a size of 35 mm×50 mm×2 mm. These samples were ground with 800 grit SiC papers to ensure the same surface roughness.

Two types of phosphate baths designated as Bath 1 and Bath 2 were used (Table 1). In Bath 1, zinc ions in the form of zinc nitrate were added to favor the formation of a crystalline film of tertiary zinc phosphate (hopeite). Fluoride ions were added as an activation agent [16]. The pH value of the bath was adjusted to approximately 2.5 with phosphoric acid. The samples

were treated in Bath 1 at 55 ℃ for 20 min. In Bath 2, calcium ions in the form of calcium nitrate were added. The processing parameters were the same as that in Bath 1.

The surface morphologies of the coatings were observed by means of scanning electron microscopy (SEM, JSM-64660LV) equipped with energy dispersive X-ray spectroscopy (EDS). The chemical compositions were analyzed with EDS. X-ray photoelectron spectroscopy (XPS, ESCAL AB250) with an Mg K_α radiation with a power of 300W was employed to make surface analysis. In addition, the phosphate coatings were analyzed using X-ray diffraction (XRD) with a Cu target.

The corrosion rates of coatings in 3.5 wt. % NaCl solutions were evaluated at room temperature. The corrosion tests were performed on a potentiostat (EG & G 273) using a classical three electrodes cell with: platinum as counter electrode, saturated calomel electrode (SCE) as reference electrode, and the sample with an exposed area of 2.84 cm^2 as working electrode. The scan rate and scan voltage range are 0.5 mVs^{-1} and ± 300 mV, respectively. All the potentials referred to in this paper are relative to the SCE.

3 Results

3.1 Micrtostructure and composition

The surface morphologies of Zn and Zn-Ca coatings are shown in Fig.1a and Fig.1b, respectively. The morphologies between these two kinds of coatings are quite different. Zn coating has two typical structures: a dry-riverbed-like or network film (marked with Spectrum 1) with micro-cracks, and randomly distributed white particles or crystals (indicated as Spectrum 2). The morphology of the Zn coating is analogous to that of the amorphous permanganate phosphate coating prepared in a bath based on manganese dihydro phosphate

[8]. The formation of cracks is possibly due to the release of hydrogen via the chemical reaction during the conversion treatment and/or the consequent dehydration of the surface layer after treatment [6]. The film prepared in Bath 2 is more compact and less cracks than that in bath 1. The crystalline Zn-Ca coating displays a flower-like morphology (Fig.1.b), which is different from that of the Zn coating.

The chemical compositions of these two coatings are shown in Table.2. The film of the Zn coating (Spectrum 1 in Fig.1a) composes of the elements: F, O, Mg and a trace of P, indicating the possible existence of MgF_2 and MgO. The white particles in the coating (Spectrum 2 in Fig. 1a) enrich with O and Zn elements, and additionally contain a small quantity of P element, implying the possible existence of crystals Zn, ZnO and the hopeite ($Zn_3(PO_4)_2 \cdot 4H_2O$). In contrast to the Zn coating, magnesium and fluoride are not identified in the Zn-Ca coatings. Moreover, the Zn-Ca coating has a much higher content of phosphor. The composition analysis of Spectrum 3 demonstrates that the Zn-Ca coating mainly contains the hopeite crystals and possibly a trace of $Ca_3(PO_4)_2$.

3.2 XRD analysis

Typical X-ray spectrums for these two phosphate coatings and the substrate are shown in Fig.2. The peaks of the substrate correspond to α-Mg phase. There exists no large difference in diffraction peaks between the substrate and the Zn-coating. The latter reveals the additional weak diffraction peaks corresponding to crystal zinc and hopeite. In the Zn-Ca coating, the tetra-hydrated zinc phosphate (hopeite) is identified [9]. This result confirms that the Zn-Ca conversion coating mainly contain the hopeite crystals.

3.3 XPS analysis

The XPS results of the phosphate conversion coatings are displayed in Fig. 3. The Zn coating predominantly contains Mg, O, P, F, C and Zn elements. The Zn-Ca coating includes Ca, O, P, C, and Zn elements. The results are in good agreement with that obtained by EDS analysis. The high content of carbon detected in the film is due to the adventitious hydrocarbons from the environment, which is common for the XPS results.

The spectra of P, Zn, Ca/Mg and O are further analyzed to discuss the detailed structure of the Zn and Zn-Ca coatings. Fig. 4 shows the high resolution spectra of the major alloying elements in the Zn coating. The high resolution spectrum of P $2p_{3/2}$ can be divided into two peaks: one at 132.9 eV and another at 133.8 eV (Fig.4a), which correspond to PO_4^{3-} and HPO_4^{-}, respectively. This result proves that the conversion film has the compounds of PO_4^{3-} and HPO_4^{2-}. Fig.4b illustrates that the high-resolution spectrum of Zn2p has two peaks: one at 1021.2 eV and another at 1044.7 eV, which correspond to the hopeite and ZnO, respectively. Among them, ZnO is formed by the oxidation of the reduced crystal zinc, which will be discussed later.

$$2Zn + H_2O \rightarrow Zn(OH)_2 \downarrow \qquad (1)$$

$$Zn(OH)_2 \rightarrow ZnO + H_2O \qquad (2)$$

Both of the high-resolution spectra of Mg 1s (Fig.4c) and O1s (Fig.4d) display only one peak, which correspond to magnesium fluoride MgF_2 and MgO, respectively. The intensity of Mg 1s and O1s peaks is high owing to the existence of MgF_2 and MgO although they are not detected by XRD.

In the formation of MgF_2, an oxidation reaction occurs as follows:

$$Mg + 2H_2O \rightarrow Mg(OH)_2 + H_2\uparrow \qquad (3)$$

Since $Mg(OH)_2$ is not stable in acidic solution, further reactions should occur as follows:

$$Mg(OH)_2 + 2HF \rightarrow MgF_2 + 2H_2O \quad (4)$$

$$Mg(OH)_2 \rightarrow MgO + H_2O \quad (5)$$

The overall reaction occurs as follows [28]:

$$Mg + H_2O + 2F^- \rightarrow MgO + MgF_2 + H_2\uparrow \quad (6)$$

In summary, based on the above analyses of EDS, XRD and XPS, it could be concluded that the Zn coating is mainly composed of four components: Zn or ZnO, MgO, MgF_2 and hopeite.

Similar to the Zn-coating, the high-resolution spectra of P $2p_{3/2}$, Zn 2p, Ca 2p and O 1s of the Zn-Ca coating are also further analyzed and discussed (Fig.5). Apparently, the spectra shown in Fig.5a and Fig.5b are analogous to that shown in Fig.4a and Fig.4b, respectively. The high-resolution spectrum of Ca 2p can be split into two peaks as a result of spin orbit splitting: Ca $2p_{3/2}$ and Ca $2p_{1/2}$ (Fig. 5(c)). Ca $2p_{3/2}$ is the satellite peak and Ca $2p_{1/2}$ the energy peak. The Ca $2p_{3/2}$ peaks at 347.8 and 346.9 eV can be attributed to calcium hydrogen phosphate hydrate $CaHPO_4 \cdot 2H_2O$ and tricalcium phosphate $Ca_3(PO_4)_2$, respectively, which are coincident with the analysis of P2p. The high-resolution spectrum of O 1s can be divided into three peaks: first at 530.0 eV, second at 531.2 eV and third at 532.1 eV (Fig. 5(d)). These three peaks correspond to ZnO, $Zn_3(PO_4)_2 \cdot 4H_2O$ and $Ca_3(PO_4)_2$, respectively. In summary, the Zn-Ca coating mainly contains $Zn_3(PO_4)_2 \cdot 4H_2O$ with a small quantity of Zn/ZnO, $Ca_3HPO_4 \cdot 2H_2O$ and $Ca_3(PO_4)_2$.

3.4 Corrosion resistance

Fig. 6 presents the polarization curves of AZ31 alloy with and without the phosphate

conversion coatings in 3.5 wt. % NaCl solution. The interesting data are listed in Table 3. The free corrosion potential increases from -1.527 for the substrate to about -1.49 V for the AZ31 alloy with phosphate coatings. The corrosion current density (i_{corr}) of the substrate, the Zn coating and the Zn-Ca coating are 242.9 μA/cm^2, 41.8 μA/cm^2 and 11.5 μA/cm^2, respectively (Table 3). This result indicates that the coatings can remarkably reduce the corrosion current density. In comparison with the Zn coating, the Zn-Ca coating improves the corrosion resistance of the AZ31 alloy more effectively.

4 Discussion

The microstructural characteristic of conversion coatings depends on the bath components and their compositions. The Zn-Ca coating is denser and has much fewer cracks than the Zn coatings. The difference in their surface morphologies is ascribed to the introduction of calcium ions, which leads to the crystallizing of the phosphate conversion coating.

Both the components and morphology of the present Zn-Ca coating are different from that reported in the previous literatures [17, 23]. Song [17] prepared a conversion film in the bath contained Ca $(NO_3)_2$ 25 g/l, $NH_4H_2PO_4$ 25 g/l at a pH value of 3.0. The chemical components of the conversion film includes calcium hydrogen phosphate dihydrate $CaHPO_4{\cdot}2H_2O$, tricalcium phosphate $Ca_3(PO_4)_2$ and magnesium phosphate $Mg_3(PO_4)_2$. As shown in Table 4, $MgHPO_4$ is slight soluble in aqueous solution, it was not involved into the conversion film. The conversion film consists of a large number of leaf-like particles and exhibits a lamellar structure. Liu found that the coating on the surface of AZ91D has a dry-riverbed-like morphology without any crystalline particles which was fabricated in the bath of manganate, phosphate, fluoride and Ca $(NO_3)_2$ [23]. Therefore, even for the Zn-Ca coatings, the

difference in the chemical compositions of the baths results in the large discrepancy in their morphology, structure and constituents.

The hydrogen evolvement can occur at β phase ($Mg_{17}Al_{12}$) in AM60 and AZ91D alloys because β phase is regarded as the microcathode [12,18]. The present substrate alloy is AZ31 alloy. There exists no β phase besides some AlMnSi particles in this alloy, which were identified by EDS (Fig.7a and Fig.7b). After this alloy was immersed into the acidic solution with pH=2.5 (solution in Bath 2) for 5 s, it started to corrode quickly. The AlMnSi particles with a higher potential act as the cathode, and the α-Mg with a lower potential as the anode:

Anode reaction:

$$Mg \rightarrow Mg^{2+} + 2e^{-} \qquad (7)$$

Hydrogen is given out from AlMnSi microcathode,

$$H_2O \rightarrow OH^{-} + H^{+} \qquad (8)$$

$$2H + 2e^{-} \rightarrow H_2 \qquad (9)$$

The microcathode reaction (Eq. (8)) results in an increase of pH value in local area near the AlMnSi particles, which facilitates the precipitation of insoluble phosphates $Mg_3(PO_4)_2$, $Ca_3(PO_4)_2$ and $Zn_3(PO_4)_2$ (Table 4) [12,18]. Due to the large amount of released magnesium ions, the compound $Mg_3(PO_4)_2$ precipitates preferentially (Fig.7c) in advance of $Ca_3(PO_4)_2$ and $Zn_3(PO_4)_2$, although the latter has a lower solubility product constants. After immersion in Bath 2 for 15s, more severe attacks occur on the surface (Fig. 8a). The compounds $Ca_3(PO_4)_2$ and $Zn_3(PO_4)_2$ are formed (Fig. 8b and Fig. 8c).

Table 5 lists the related thermodynamic data. The change in Gibbs free energy ΔG of the phosphates $Ca_3(PO_4)_2$ and $Zn_3(PO_4)_2$ is -187.71 kJ/mol and -186.33 kJ/mol, respectively.

These two values are really close, indicating that both calcium phosphate and zinc phosphate can simultaneously precipitate on the surface:

$$Ca^{2+} + HPO_4^- \rightarrow CaHPO_4 \qquad (11)$$

$$CaHPO_4 \rightarrow Ca_3(PO_4)_2 + H^+ \qquad (12)$$

$$3Zn^{2+} + 2H_2PO_4^- + 2H^+ + 4H_2O + 6e^- \rightarrow Zn_3(PO_4)_2 \cdot 4H_2O + 3H_2\uparrow \qquad (13)$$

$Zn_3(PO_4)_2$•$4H_2O$ is therefore the main ingredient of the Zn-Ca coating. After the phosphate film is formed, it further acts as the microcathode. During phosphating process in the areas of microcathode, Zn^{2+} ions becomes zinc by absorbing the electrons and deposits on the surface [18]:

$$Zn^{2+} + 2e^- \rightarrow Zn \qquad (14)$$

Consequently, zinc was detected by XRD in both Zn and Zn-Ca coatings.

The growth of few nuclei of calcium phosphate and zinc phosphate leads to the formation of flower-like phosphates after immersion for 30 s (Fig.9a). About one third of the film is covered by these flower-like phosphates after immersion for 1.5 min (Fig.9b). After immersion for 5 min, the film is completely covered by these flower-like phosphates (Fig.9c). The surface morphology has no obvious variation with further increasing the immersion time from 10 to 30 min (Fig. 9d-f). The formed phosphates are considered as the hopeite after immersion for more than 20 min, because EDS analysis shows that the Zn-Ca coating contains no magnesium and calcium (Table 6).

Based on the above discussion, a model is proposed to explain the formation of the Zn-Ca coating (Fig.10). The formation of the Zn-Ca coating follows four steps: (1) dissolution of magnesium and evolution of hydrogen (Fig.10a), (2) nuclei formation of magnesium phosphate (Fig.10b), (3) nuclei formation of calcium phosphate and zinc phosphate (Fig.10c)

and (4) growth of the crystalline zinc phosphate (Fig.10d).

5. Conclusions

1) The Zn-Ca coating has a flower-like morphology, which is different from Zn coating with a dry-riverbed-like morphology. The Zn-Ca coating is denser with almost no cracks than Zn coatings.

2) The Zn coating contains Zn/ZnO, MgO, MgF_2 and $Zn_3(PO_4)_2{\cdot}4H_2O$. The Zn-Ca coating is mainly composed of $Zn_3(PO_4)_2{\cdot}4H_2O$, and a small quantity of ZnO, $Ca_3(PO_4)_2$ and $CaHPO_4$.

3) The formation of the Zn-Ca coating follows four steps: (1) dissolution of magnesium and evolution of hydrogen, (2) nuclei formation of magnesium phosphate, (3) nuclei formation of calcium phosphate and zinc phosphate and (4) growth of the crystalline zinc phosphate.

4) Both Zn coating and Zn-Ca coating are corrosion resistant than the substrate alloy. In comparison with the former, the latter Zn-Ca coating can reduce the corrosion current density more significantly.

Acknowledgements

The work was financially supported by Key technologies R & D Program of Chongqing CSTC, 2009AB4008.

References:

[1] R.C.Zeng, J. Zhang, W.J. Huang, W. Dietzel, K.U. Kainer, C. Blawert, W. Ke, T. Nonferr. Metal Soc. 16 (2006) s763-s771.

[2] G. Song, A. Atrens, Adv. Eng. Mater. 7 (2005) 837-858.

[3] Z.M. Shi, G.L. Song, A. Atrens, Corros. Sci. 48 (2006) 3531-3546.

[4] Y.W. Song, D.Y. Shang, R.S. Chen, E.H. Han, Surf. Eng. 23 (2007) 334-338.

[5] F.W. Eppensteiner, M.R. Jenkins, Metal Fin. 100 (2002) 479-491.

[6] Z.C. Kwo, S.S. Teng, Mater. Chem. Phys. 80 (2003) 191-200.

[7] G. Y. Li, J.S. Lian, L.Y. Niu, Z.H. Jiang. Adv. Eng. Mater. 8 (2006) 123-127.

[8] W.Q. Zhou, D.Y. Shan, E.H. Han, W. Ke, Corros. Sci. 50 (2008) 329-337.

[9] L. Kouisni, M. Azzi, M. Zertoubi, F. Dalard, S. Mazimovitch, Surf. Coat. Tech. 185 (2004)58-67.

[10] X.F. Cui, Y. Li, Q.F. Li, G. Jin, M.H. Ding, F.H. Wang, Mater. Chem. Phys. 11 (2008) 503–507.

[11] M. Dabala, K. Brunelli, E. Napolitani, M. Magini, Surf. Coat. Tech. 172 (2003) 227-232.

[12] J.E. Gray, B. Luan, J. Alloy Compd. 336 (2002) 88-113.

[13] R.C. Zeng, Z.D. Lan, J. Chen, X.H. Mo, E.H. Han, The Chinese Journal of Nonferrous Metals 19 (2009) 397-404.

[14] F. Zucchi, A. Frignani, V. Grassi, G. Trabanelli, C. Monticelli, Corros. Sci. 49 (2007) 4542-4552.

[15] G.N. Bhar, N.C. Debnath, S. Roy, Surf. Coat. Tech. 35 (1988) 171-179.

[16] L. Kouisni, M. Azzi, F. Dalard, S. Mazimovitch, Surf. Coat. Tech. 192 (2005) 239-246.

[17] Y.W. Song, D.Y. Shan, R.S. Chen, F. Zhang, E.H. Han, Surf Coat. Tech. 203 (2009) 1107-1113.

[18] L.Y. Niu, Z.H. Jiang, G.Y. Li, C.D. Gu, J.S. Lian, Surf. Coat. Tech. 200 (2006) 3021-3026.

[19] B.L. Lin, J.T. Lu, G. Kong, J. Liu, T. Nonferr. Metal Soc. 17 (2007) 755-761.

[20] D. Weng, P. Jokiel, A. Uebleis, H. Boehni, Surf. Coat. Tech. 88 (1997) 147-156.

[21] A. Albu-Yaron, Y.M. Aravot, Thin Solid Films 232 (1993) 208-214.

[22] M. Zhao, S.S. Wu, J.R. Luo, Y. Fukuda, H. Nakae, Surf. **Coat.** Tech. 200 (2006) 5407-5412.

[23] F. Liu, D.Y. Shan, E.H. Han, C.S. Liu, Chinese J. Nonferrous Met. 18 (2008) 1825-1830.

[24] Z.Y. Yong, J. Zhu, C. Qiu, Y.L. Liu, Appl. Surf. Sci. 255 (2008) 1672-1680.

[25] Q. Li, S.Q. Xu, J.Y. Hu, S.Y. Zhang, X.K. Zhong, X.K.Yang, Electrochim. Acta 55 (2010) 887-894.

[26] R.C. Zeng, Z.D. Lan, Chinese J. Nonferrous Met. 20 (2010) 1461-1466.

[27] E.H. Han, W.Q. Zhou, D.Y. Shan, W. Ke, Mat. Sci. Forum 419-4 (2003) 879.

[28] T.T. Yan, L.L. Tan, D. S. Xiong, X.J. Liu, B.C. Zhang, K. Yang, Mater. Sci. Eng. C, 30 (2010) 740-748.

[29] C.W. Hu, Chemistry, Chemical Industry Press, 2004.

Figure captions:

Fig.1 SEM micrographs showing the morphologies of coatings, (a) Zn coating and (b) Zn-Ca coating.

Fig. 2 X-ray diffraction spectra of the coatings formed on magnesium alloy.

Fig. 3 XPS spectra of conversion coating, (a) Zn coating and (b) Zn-Ca coating.

Fig. 4 XPS spectra for the Zn-coating, (a) P $2p_{3/2}$, (b) Zn 2p, (c)Mg 1s, (d) O 1s.

Fig. 5 XPS spectra for the Zn-Ca coating, (a) P $2p_{3/2}$, (b) Zn 2p, (c) Ca 2p, (d) O 1s.

Fig. 6 Polarization curves for the coatings and AZ31 alloy.

Fig.7 (a) Surface morphologies of the alloy after immersion for 5s in Bath 2, (b) AlMnSi particles, and (c) precipitate of magnesium phosphate.

Fig. 8 (a) Surface morphologies of the alloy after immersion for 15s in Bath 2; nuclei formation of (b) zinc and calcium phosphate, and (c) zinc phosphate.

Fig.9 Surface morphologies of the Zn-Ca coating at various soaking times: (a) 30 s, (b) 1.5 min, (c) 5 min, (d) 10 min, (e) 20 min and (f) 30 min.

Fig. 10 Schematic diagrams of the formation of Zn-Ca coating.

Table Captions:

Table 1 Chemical composition of the phosphate baths, g/L.

Table 2 Chemical compositions of the coating in different position (wt %).

Table 3 Electrochemical parameters of polarization curves.

Table 4 Solubility product constant of some compounds (298.15K) [29].

Table 5 Thermodynamics data for calcium phosphate and zinc phosphate at 298.15K. ΔH is the enthalpy change, ΔS is the entropy change, T is the absolute temperature.

Table 6 Chemical compositions of the Zn-Ca coating after immersion for long time 20 and 30 min.

4. Table(s)1

Click here to download high resolution image

Bath	Na_2HPO_4	$Zn(NO_3)_2$	$Ca(NO_3)_2$	$NaNO_2$	NaF
Bath 1	10	6	—	4	2
Bath 2	10	6	2	4	2

4. Table(s)2

Click here to download high resolution image

Locations	O	F	Mg	P	Zn	Ca
Spectrum 1	26.13	57.68	13.56	2.63	—	—
Spectrum 2	49.80	—	—	1.48	48.73	—
Spectrum 3	39.79	—	—	15.15	44.52	0.54

4. Table(s)3

Click here to download high resolution image

Sample	E_{corr}(V)	i_{corr} (μA/cm^2)
AZ31substra	-1.527	242.9
Zn coating	-1.494	41.8
Zn-Ca coatin	-1.498	11.5

4. Table(s)4

Click here to download high resolution image

Compounds	K_{sp}^{0}	Compounds	K_{sp}^{0}
$Ca(OH)_2$	5.5×10^{-6}	$MgHPO_4\cdot3H_2O$	1.5×10^{-6}
$CaHPO_4$	1.0×10^{-7}	$Mg_3(PO_4)_2$	1.0×10^{-25}
$Ca_3(PO_4)_2$	2.0×10^{-29}	$Zn(OH)_2$	1.2×10^{-17}
MgF_2	5.1×10^{-11}	$Zn_3(PO_4)_2$	9.0×10^{-33}
$Mg(OH)_2$	5.6×10^{-12}		

4. Table(s)5

Click here to download high resolution image

Compounds	ΔH (kJ/mol)	ΔS (J/k · mol)	$T\Delta S$ (kJ/mol)	ΔG (kJ/mol)
$Ca_3(PO_4)_2$	62.49	839.3	250.2	-187.71
$Zn_3(PO_4)_2$	116.97	1017.3	303.3	-186.33

4. Table(s)6

Click here to download high resolution image

Time /min	O	P	Zn
20	50.16	15.87	33.97
30	47.06	21.35	31.60

5. Figure(s)1a
Click here to download high resolution image

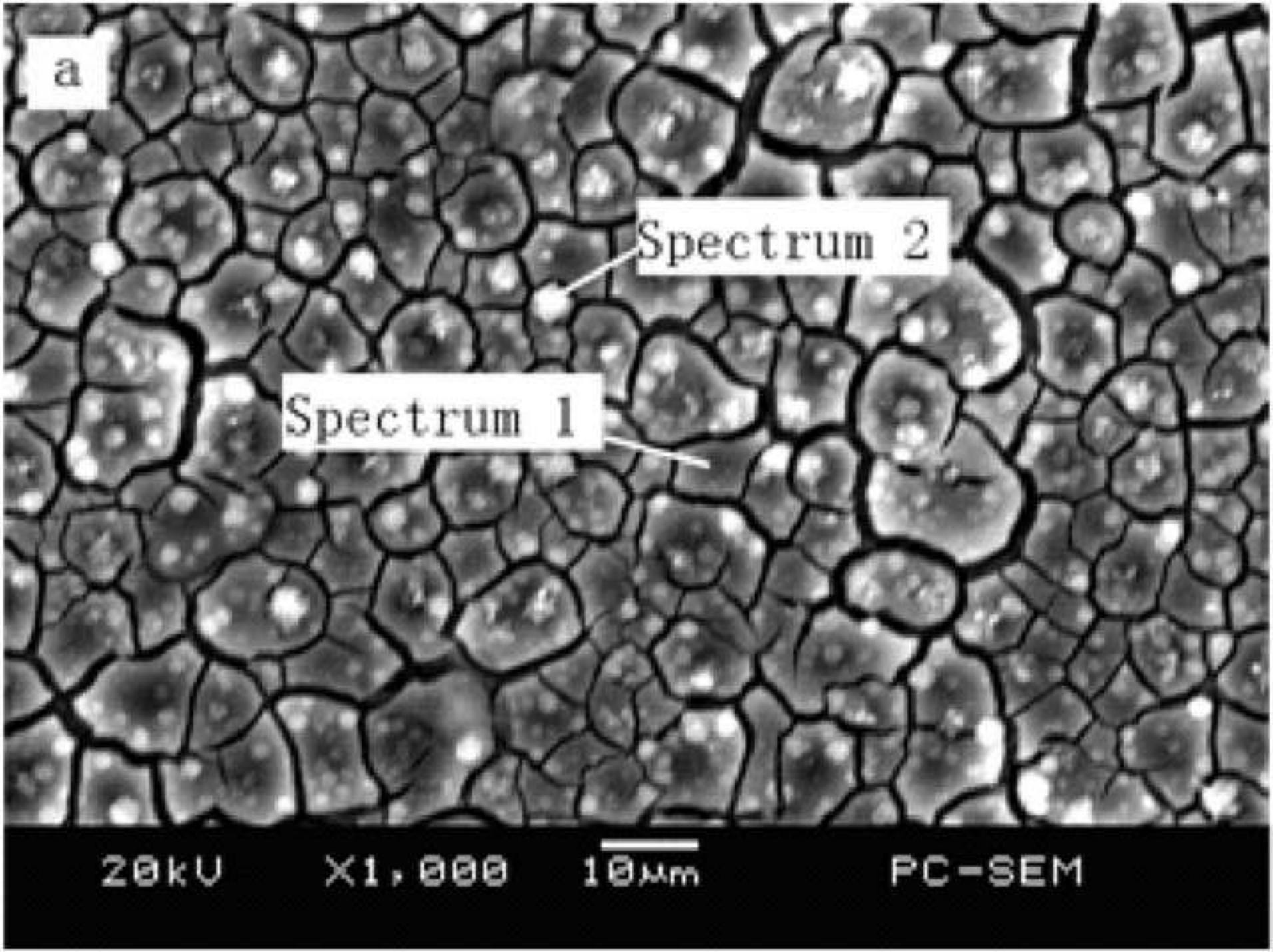

5. Figure(s)1b

Click here to download high resolution image

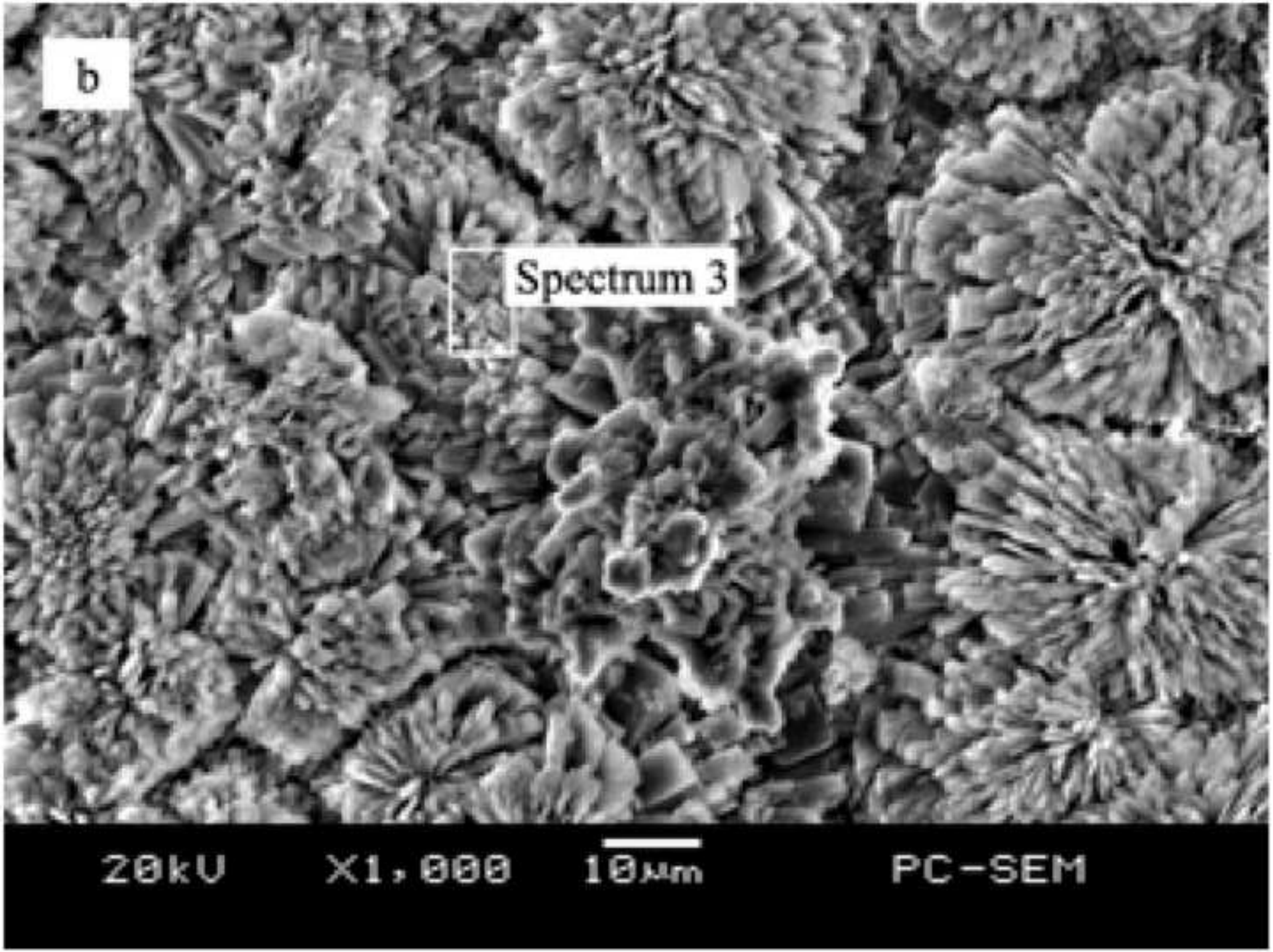

5. Figure(s)2

Click here to download high resolution image

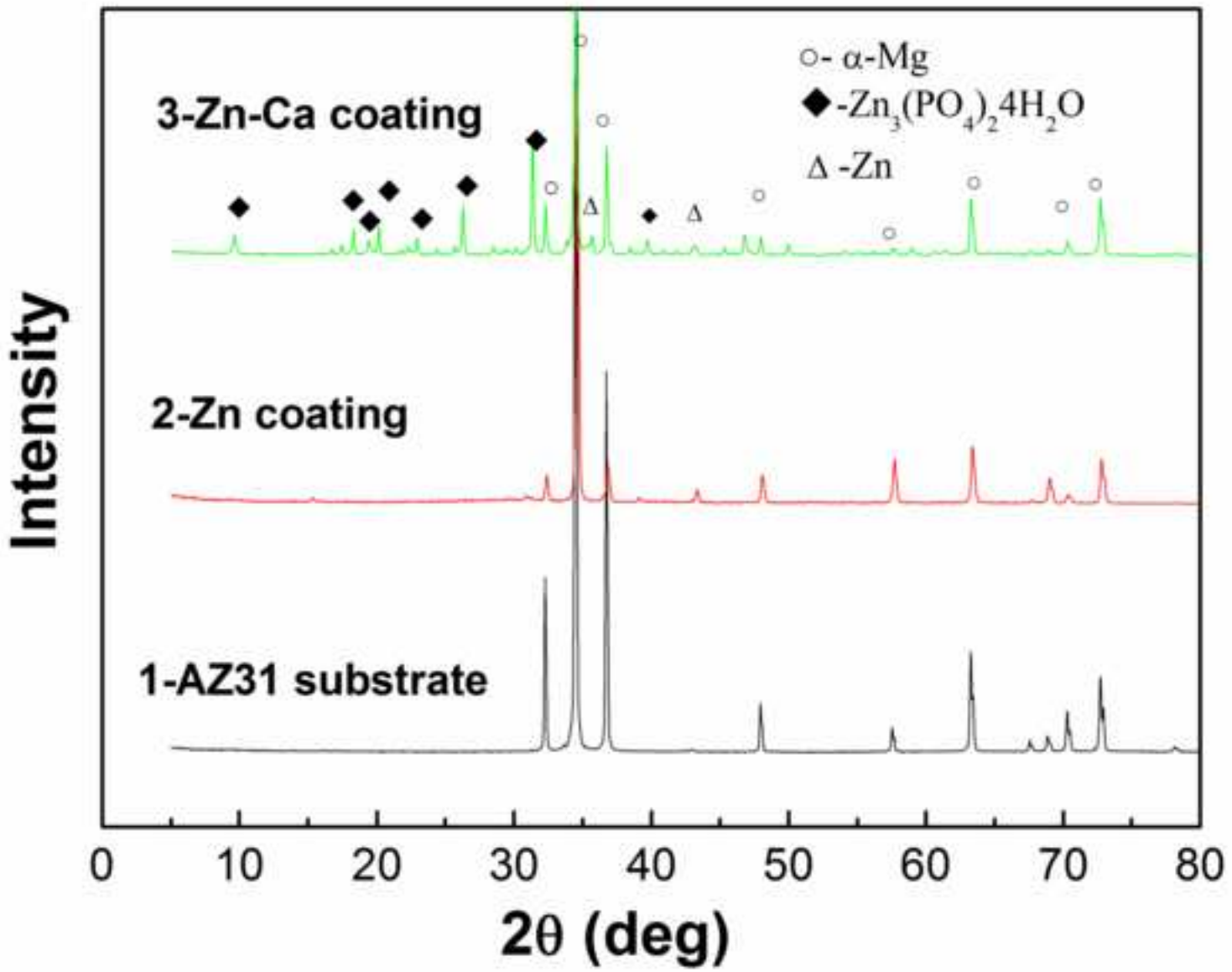

5. Figure(s)3a

Click here to download high resolution image

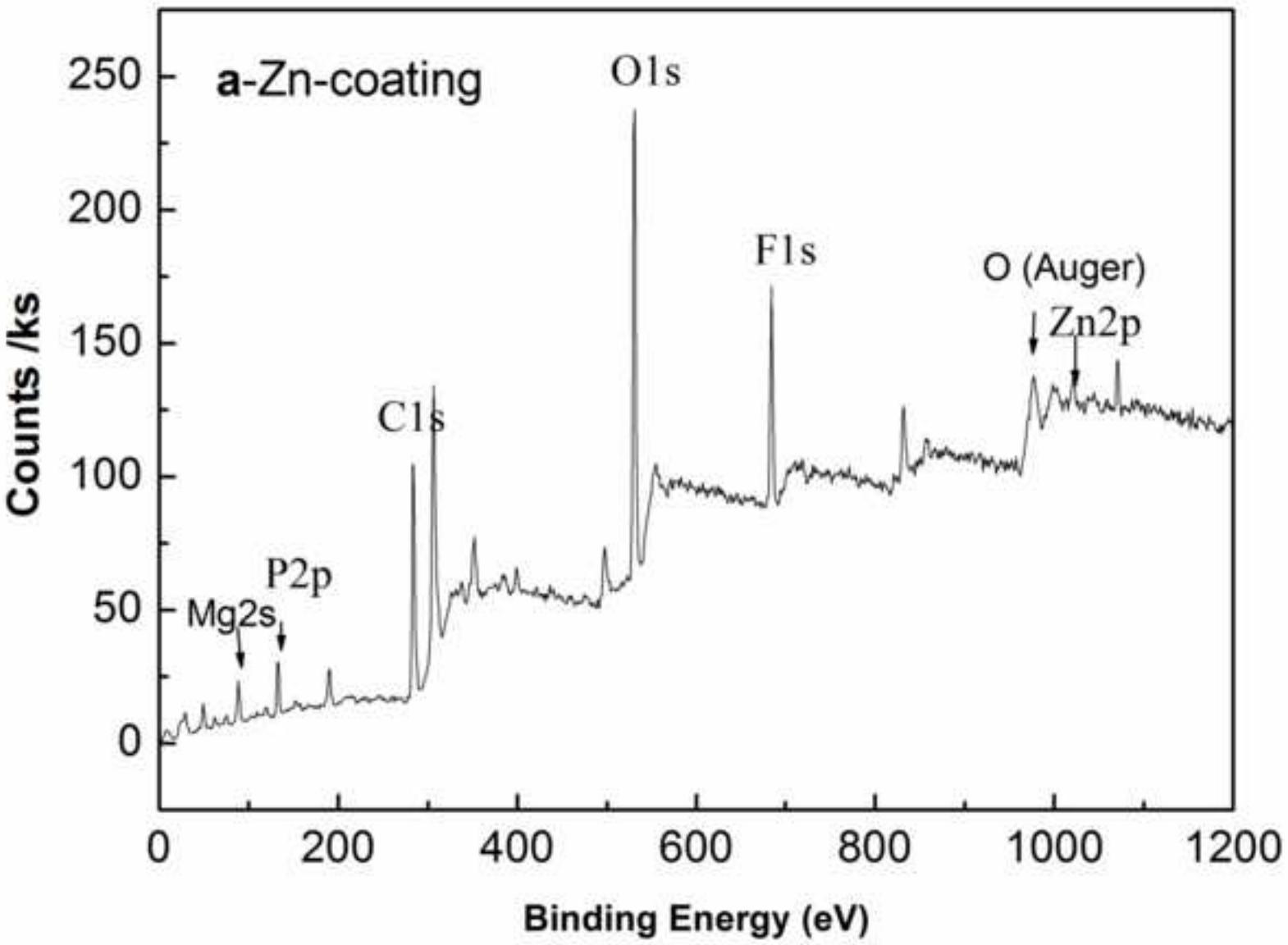

5. Figure(s)3b
Click here to download high resolution image

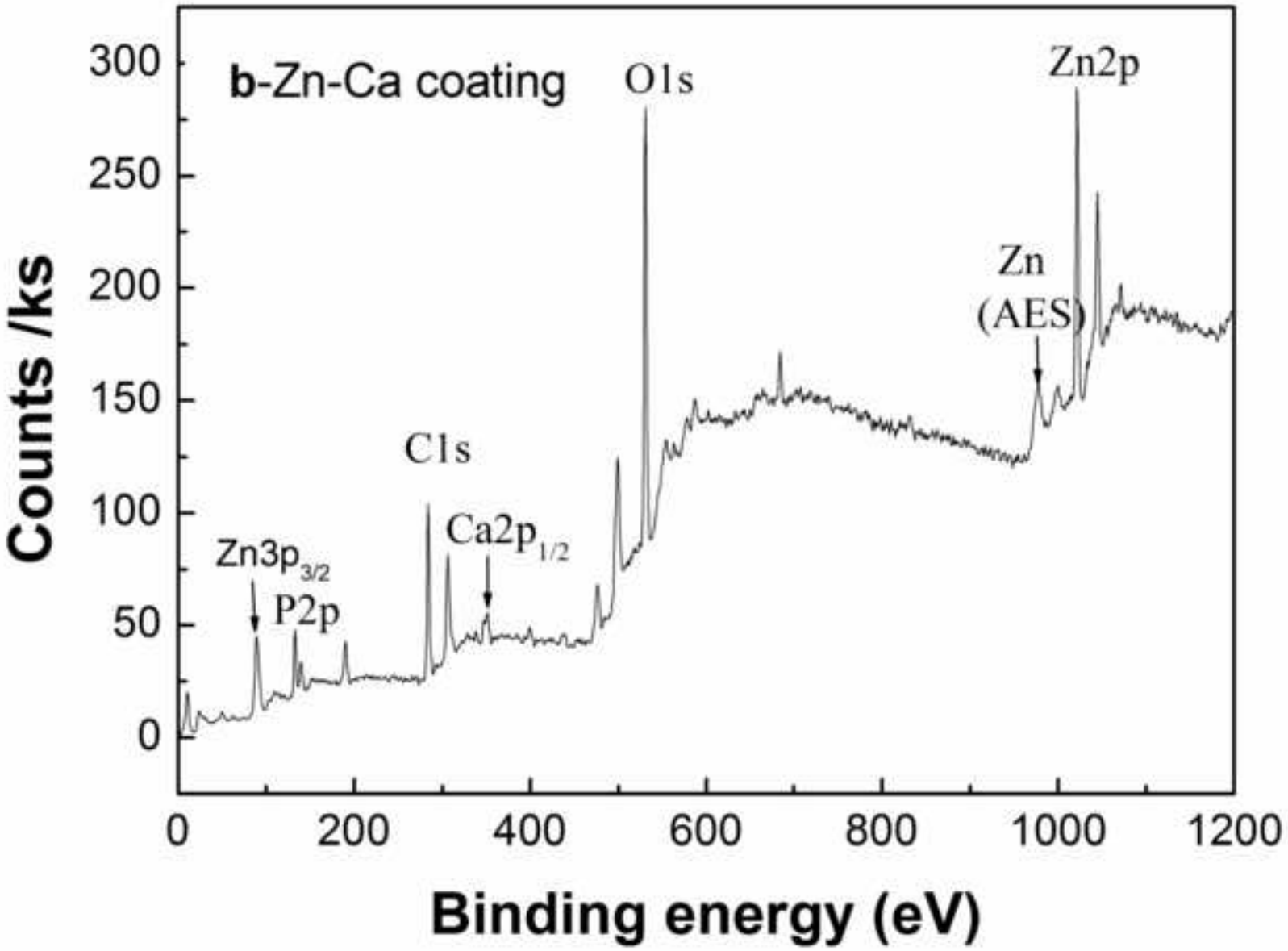

5. Figure(s)4a

Click here to download high resolution image

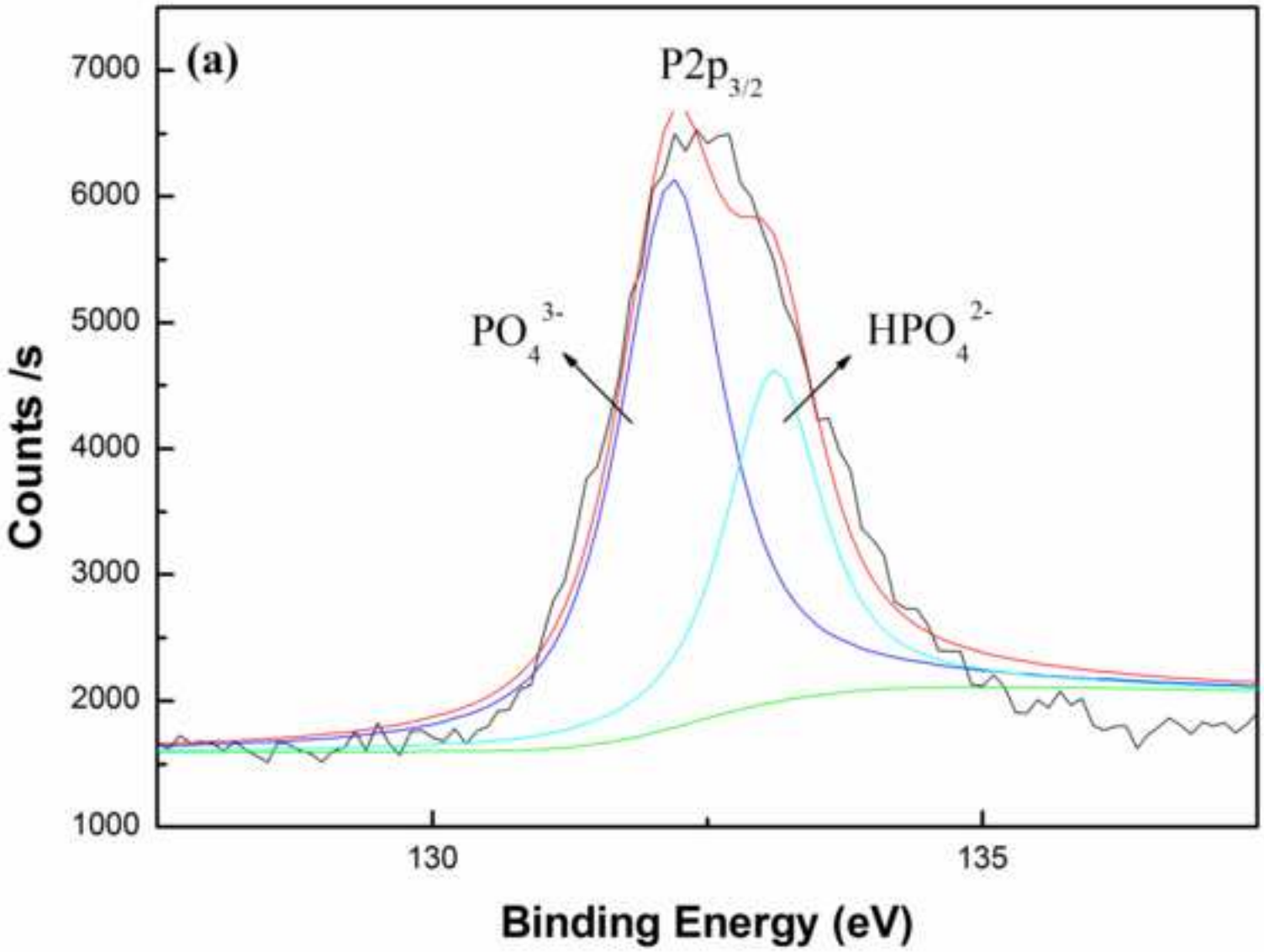

5. Figure(s)4b
Click here to download high resolution image

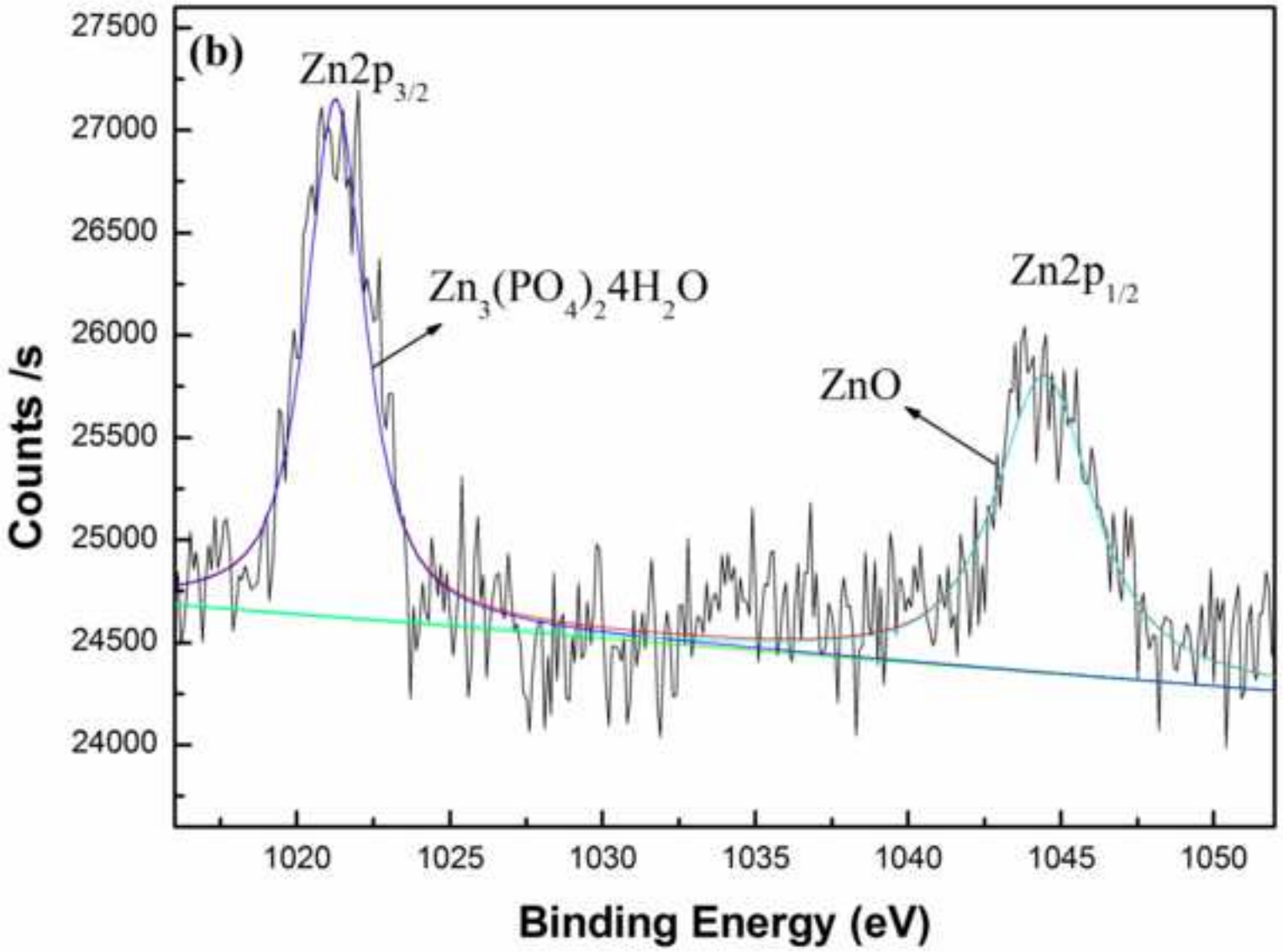

5. Figure(s)4c
Click here to download high resolution image

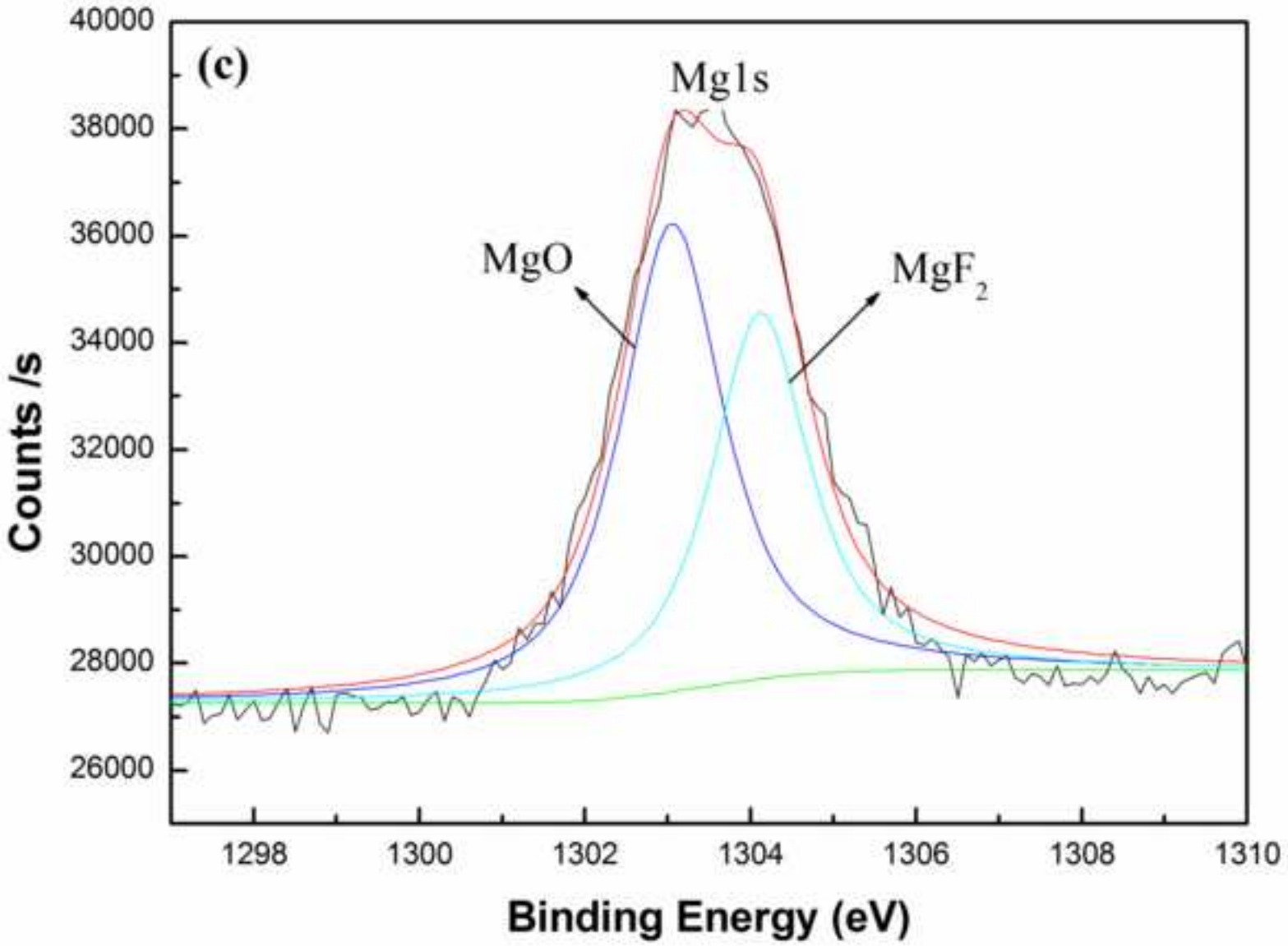

5. Figure(s)4d
Click here to download high resolution image

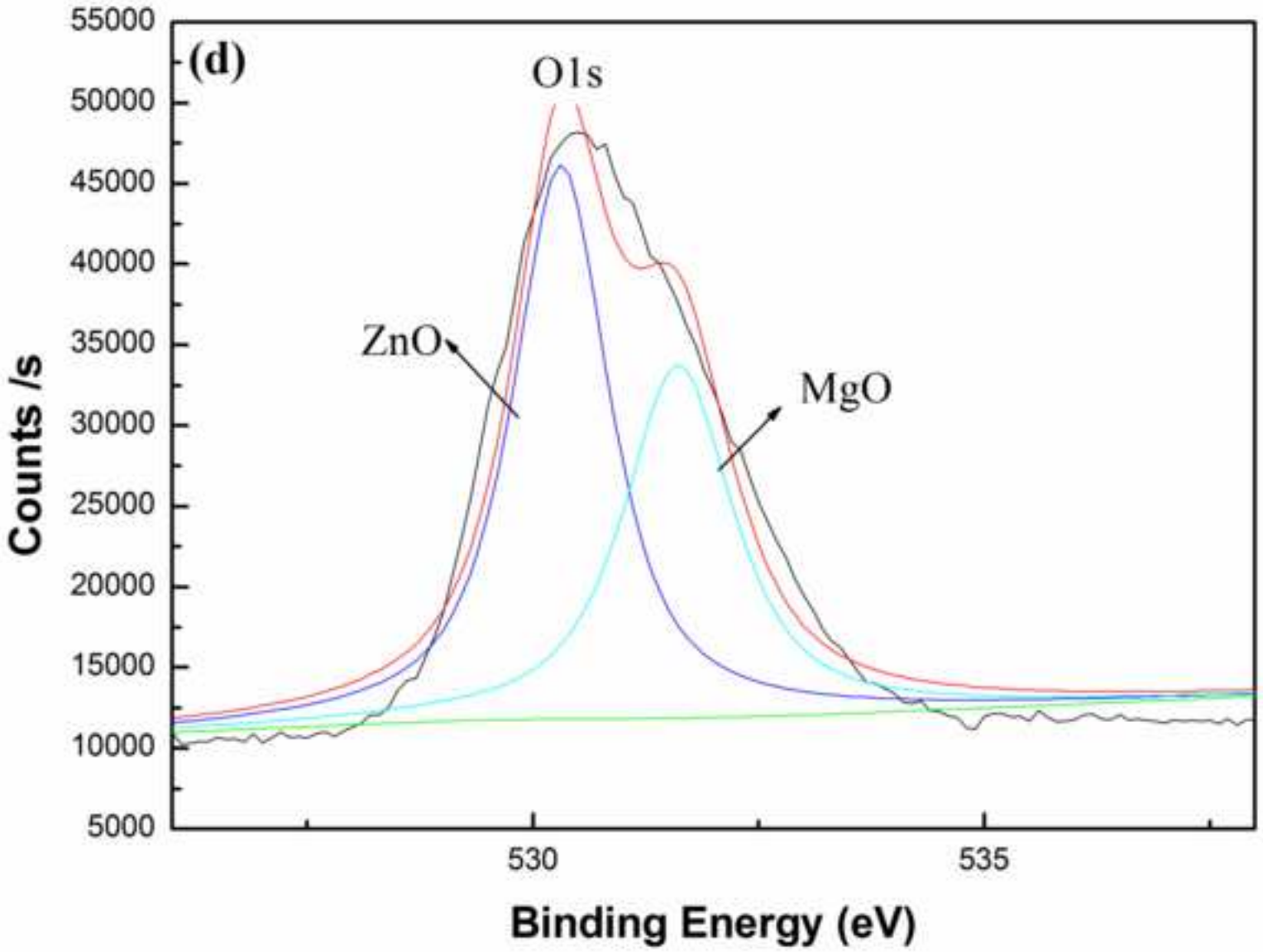

5. Figure(s)5a
Click here to download high resolution image

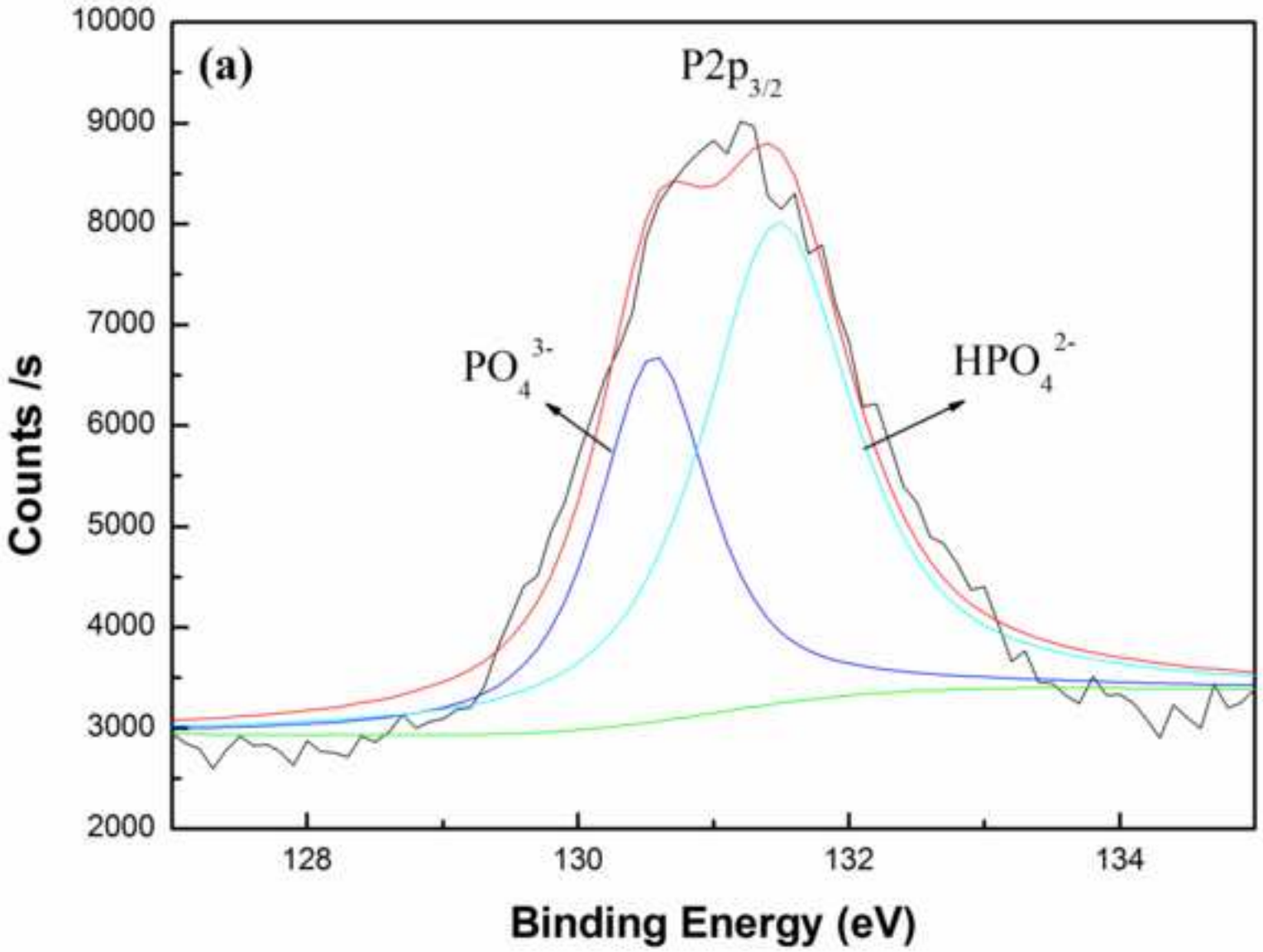

5. Figure(s)5b
Click here to download high resolution image

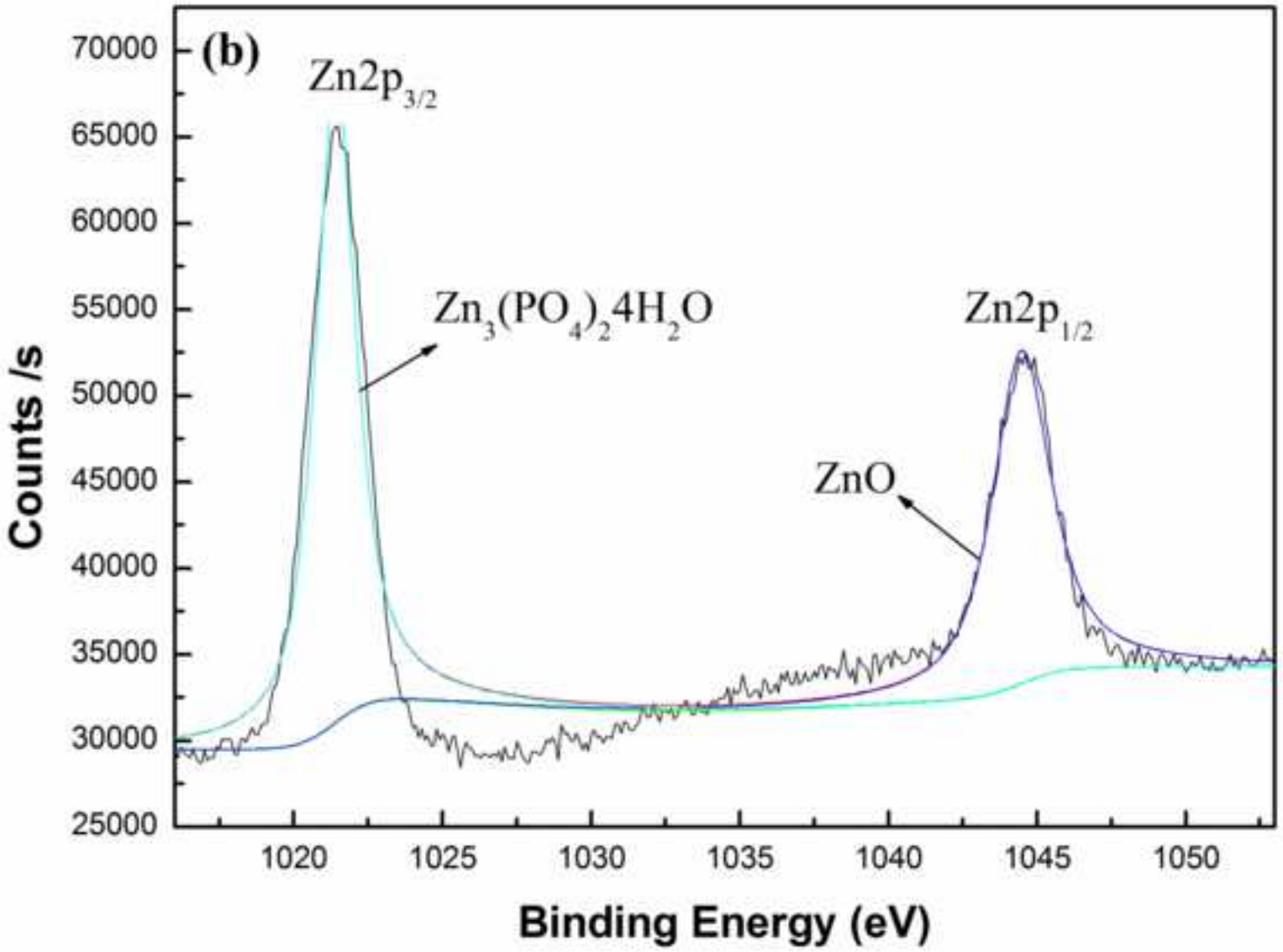

5. Figure(s)5c
Click here to download high resolution image

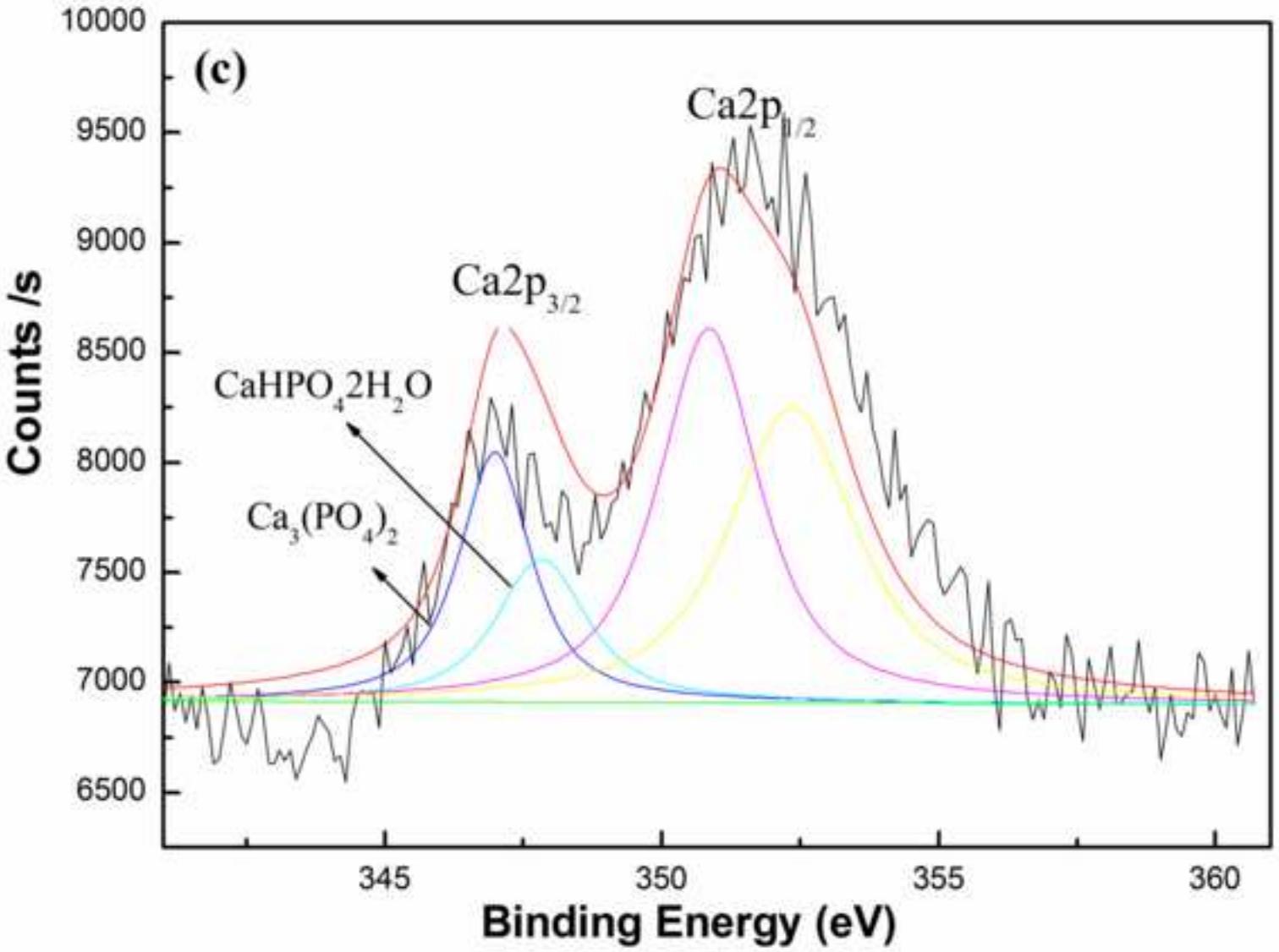

5. Figure(s)5d
Click here to download high resolution image

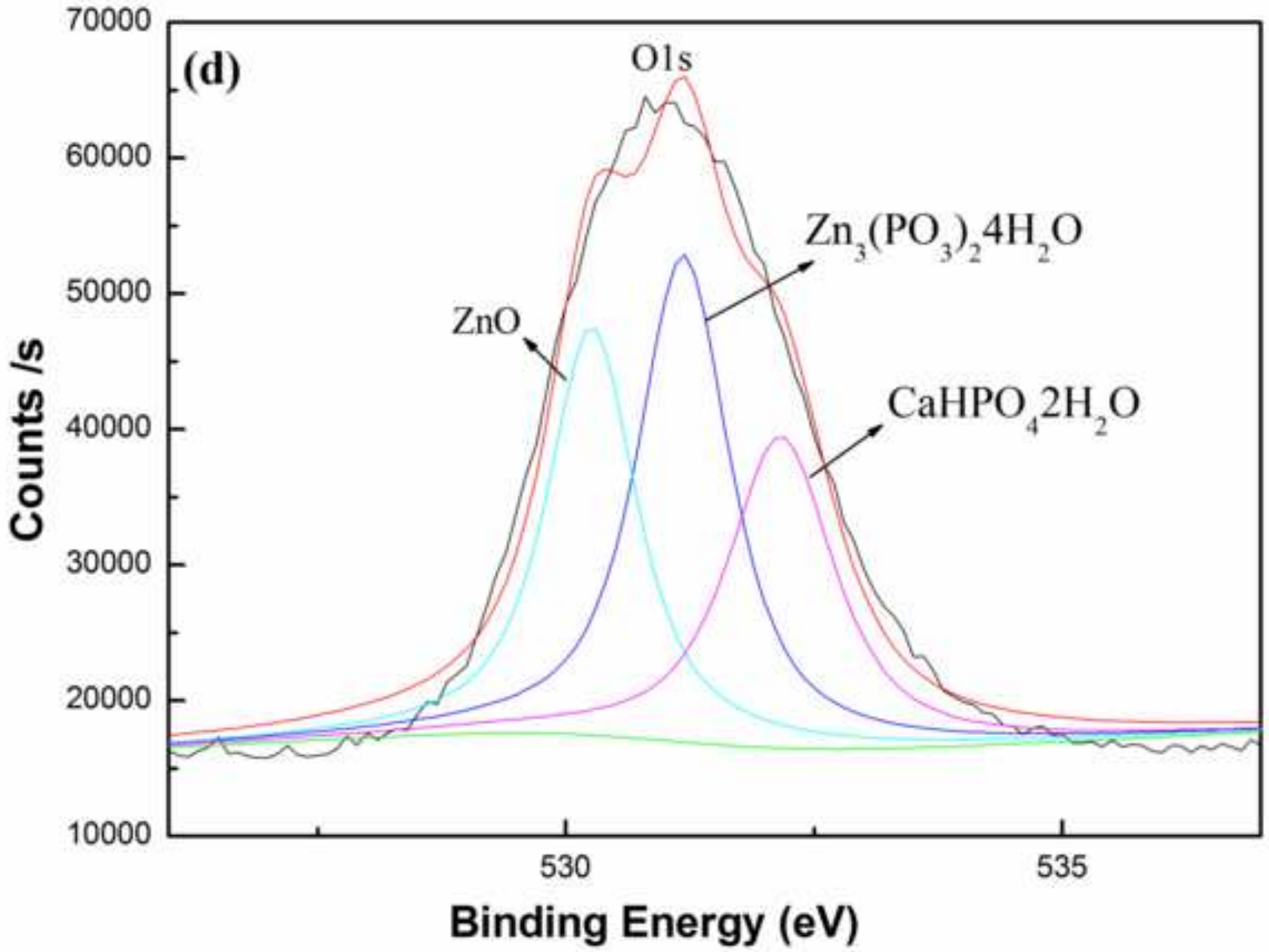

5. Figure(s)6
Click here to download high resolution image

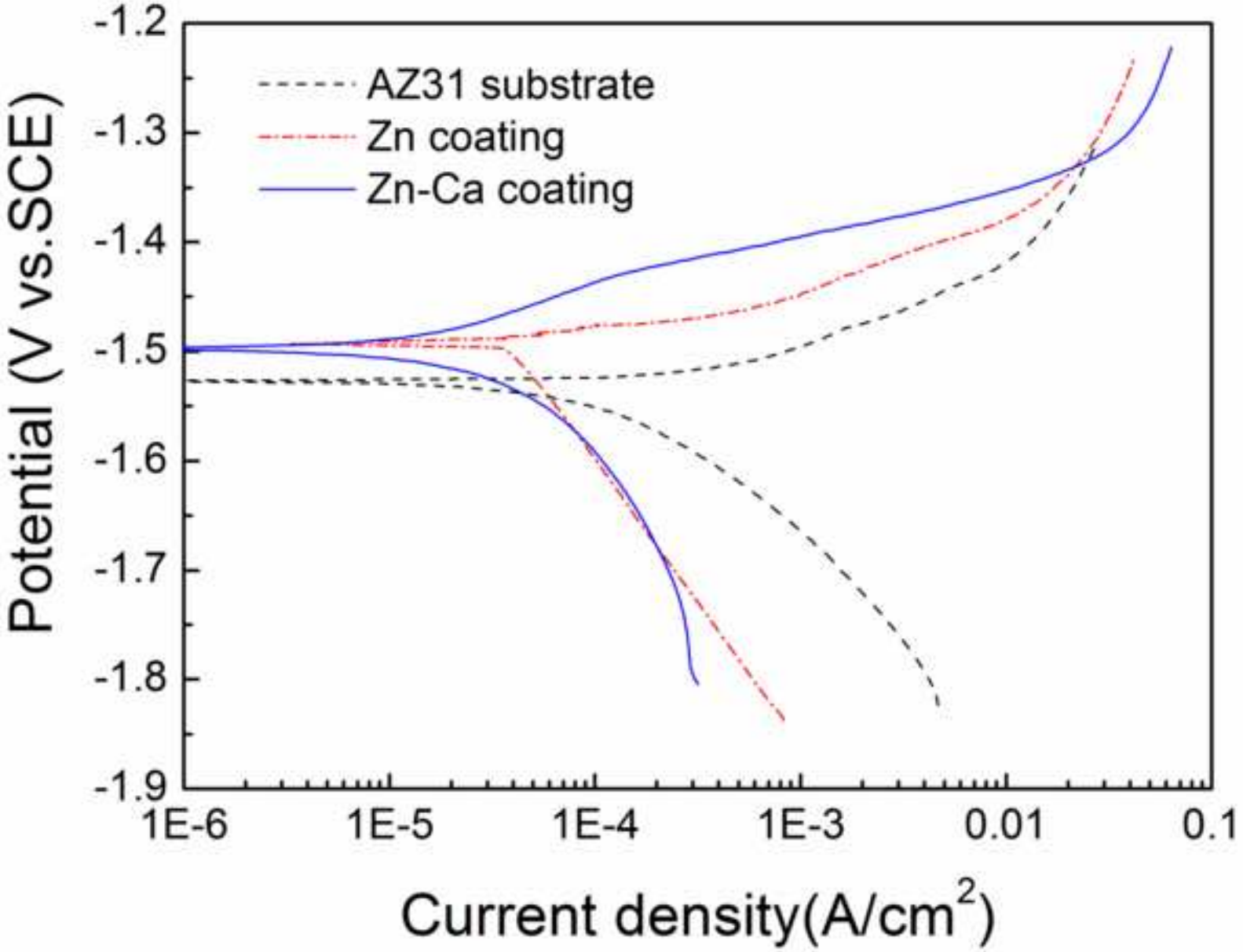

5. Figure(s)7a

Click here to download high resolution image

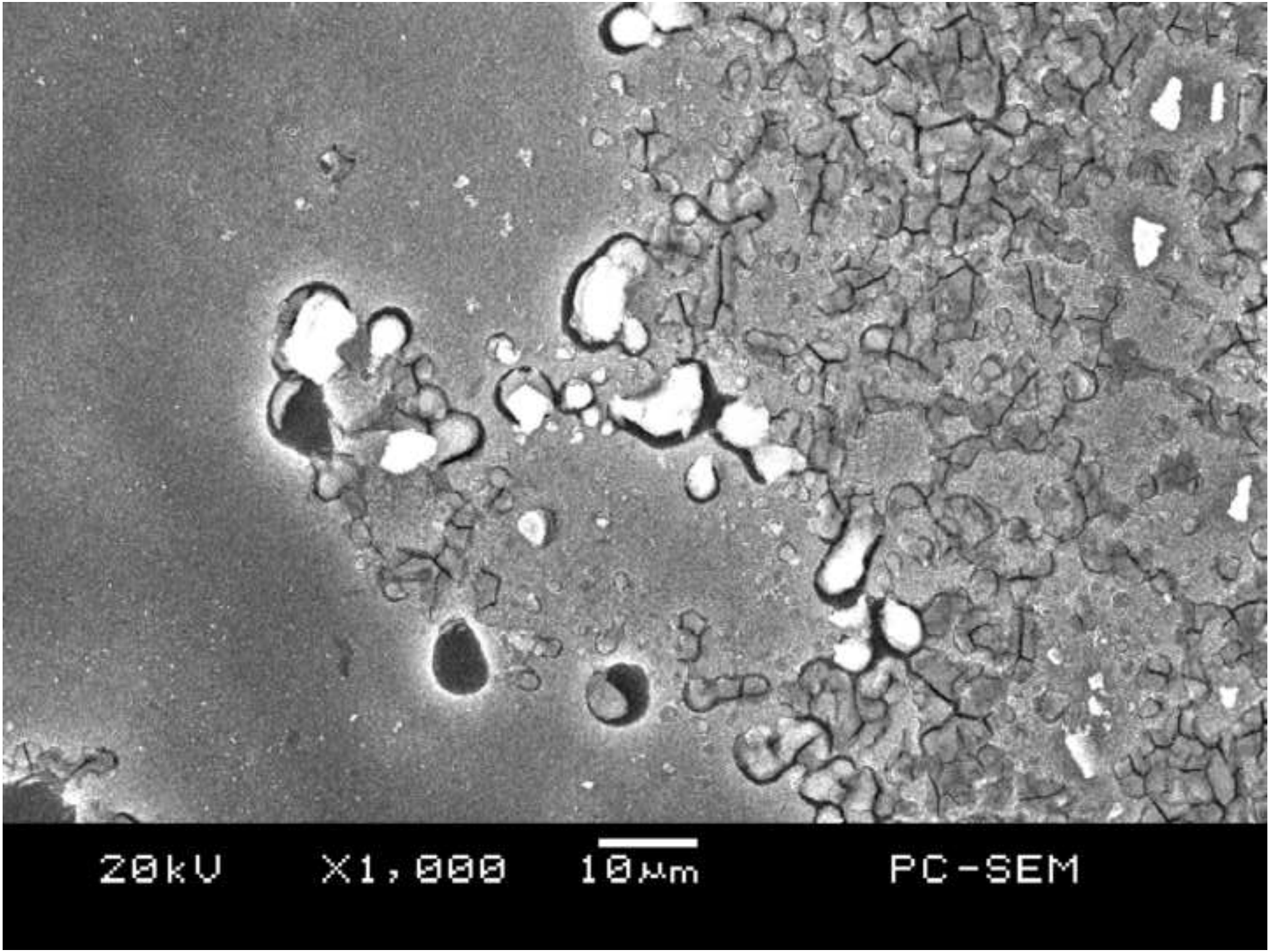

5. Figure(s)7b

Click here to download high resolution image

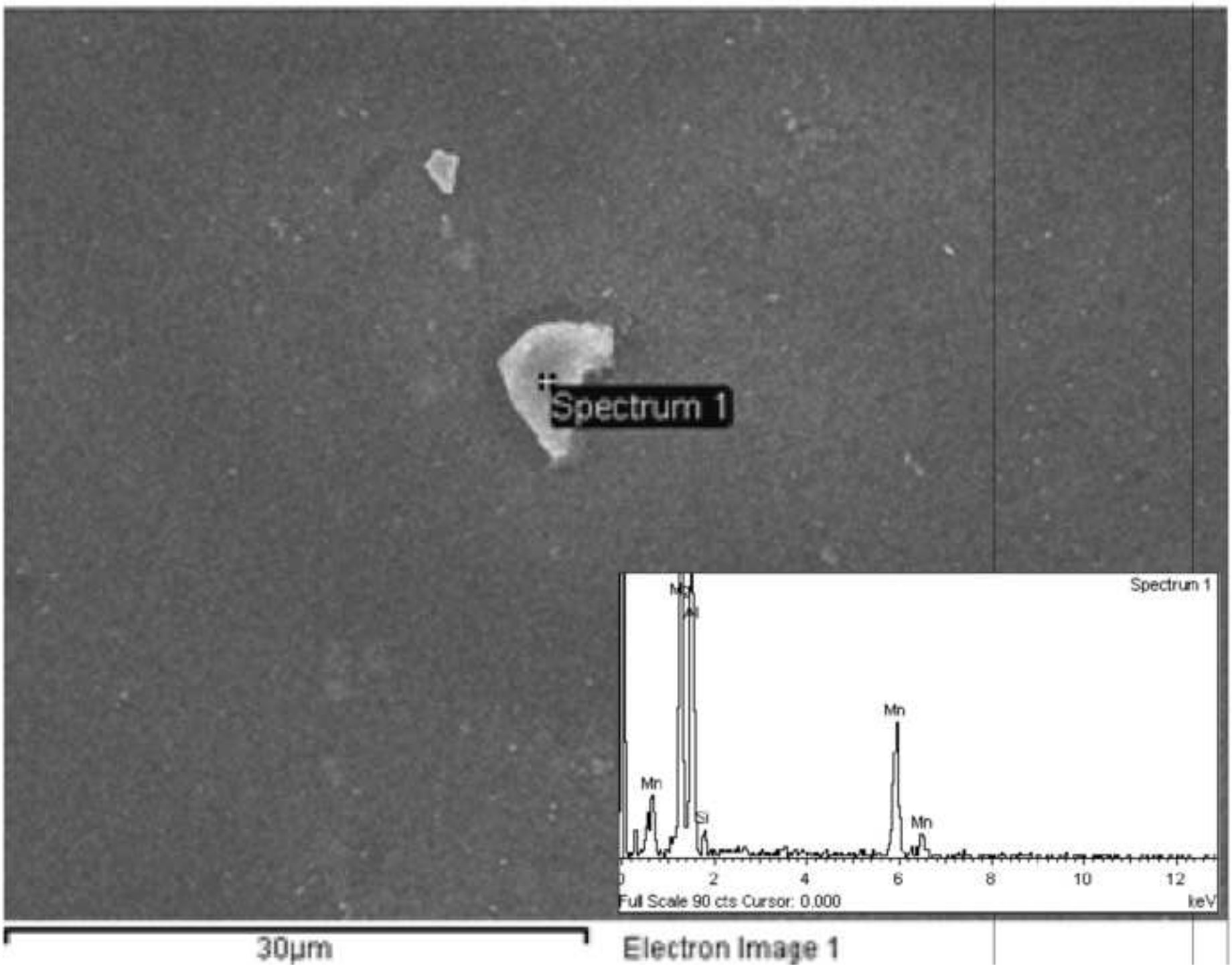

5. Figure(s)7c

Click here to download high resolution image

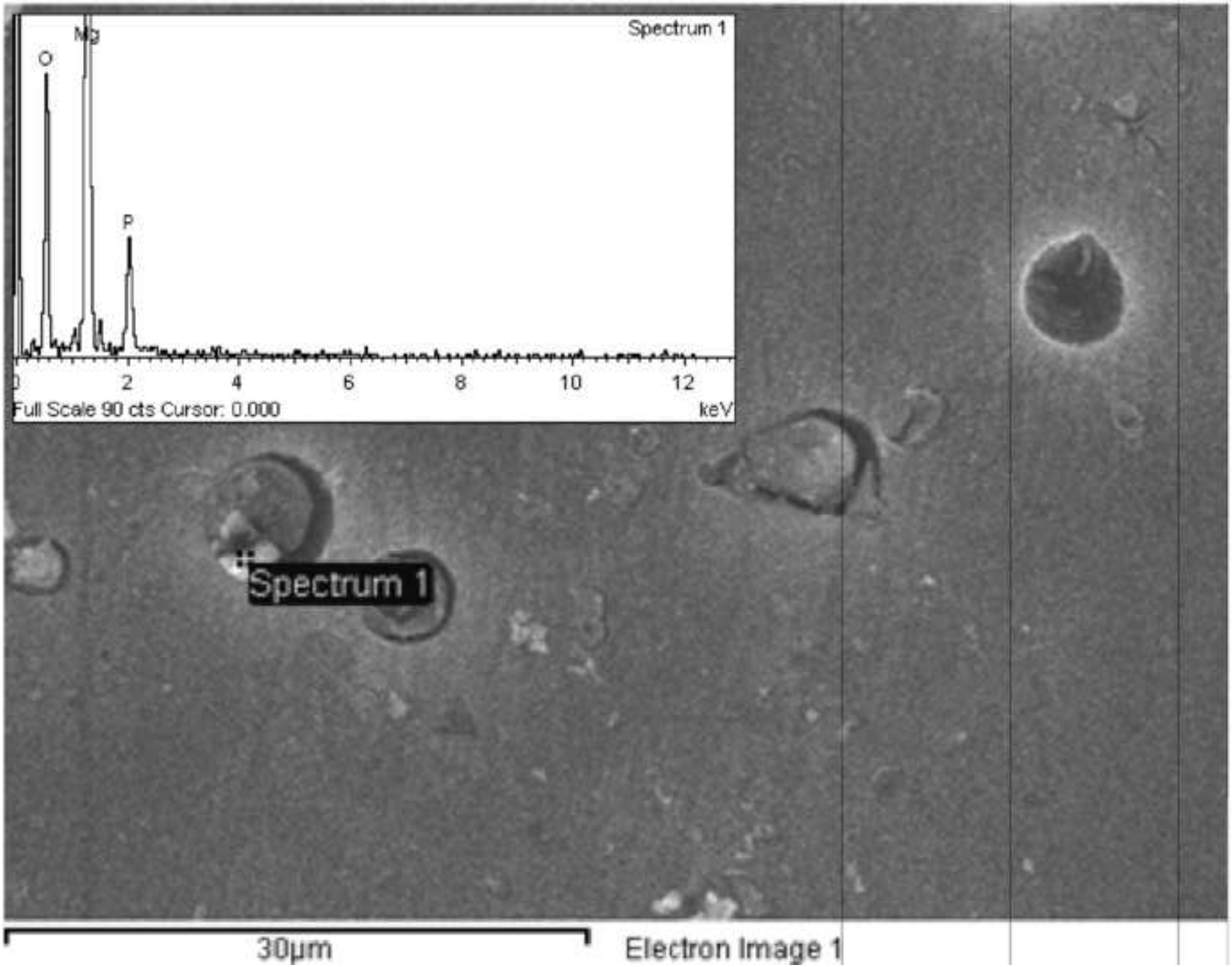

5. Figure(s)8a
Click here to download high resolution image

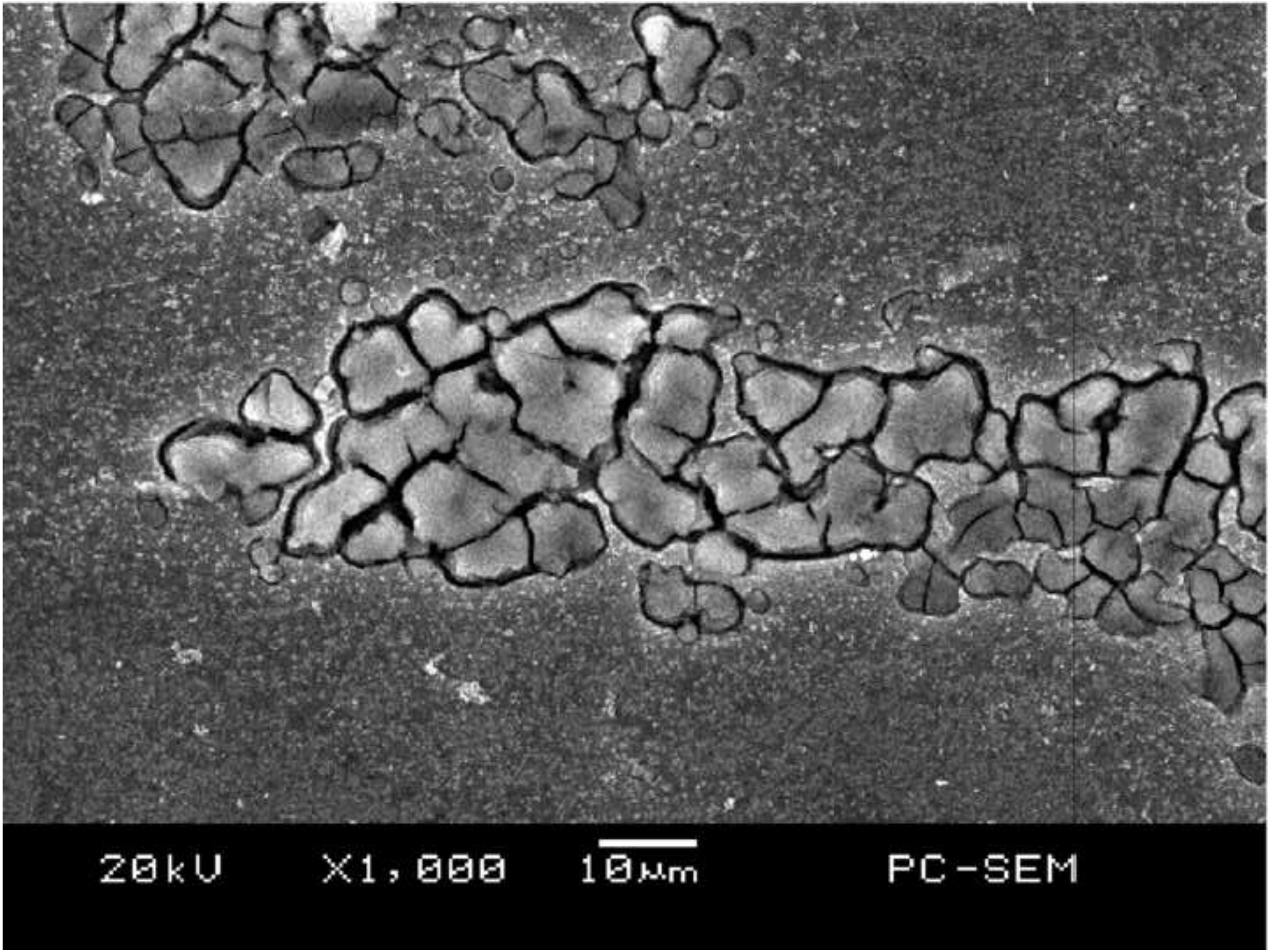

5. Figure(s)8b

Click here to download high resolution image

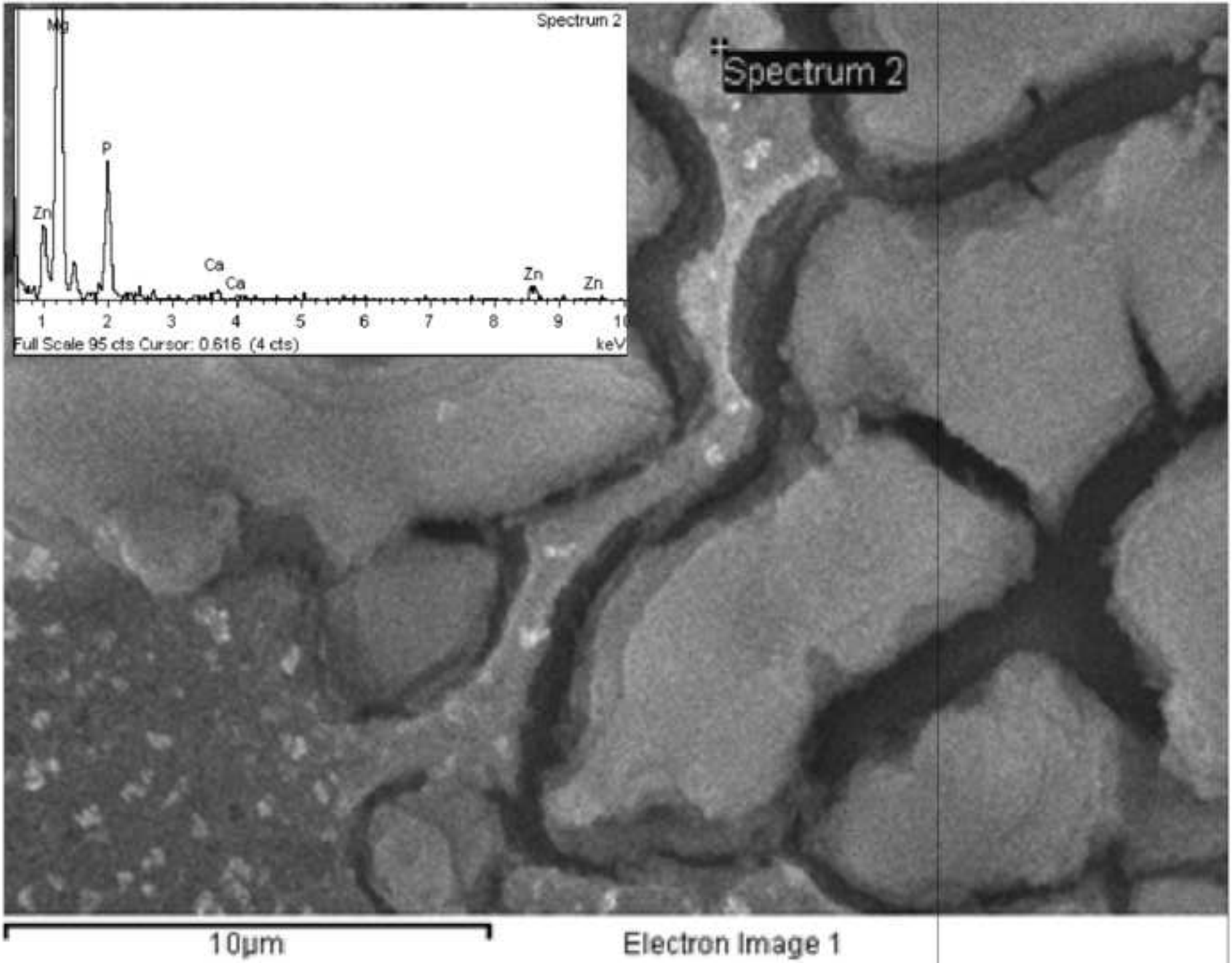

5. Figure(s)8c

Click here to download high resolution image

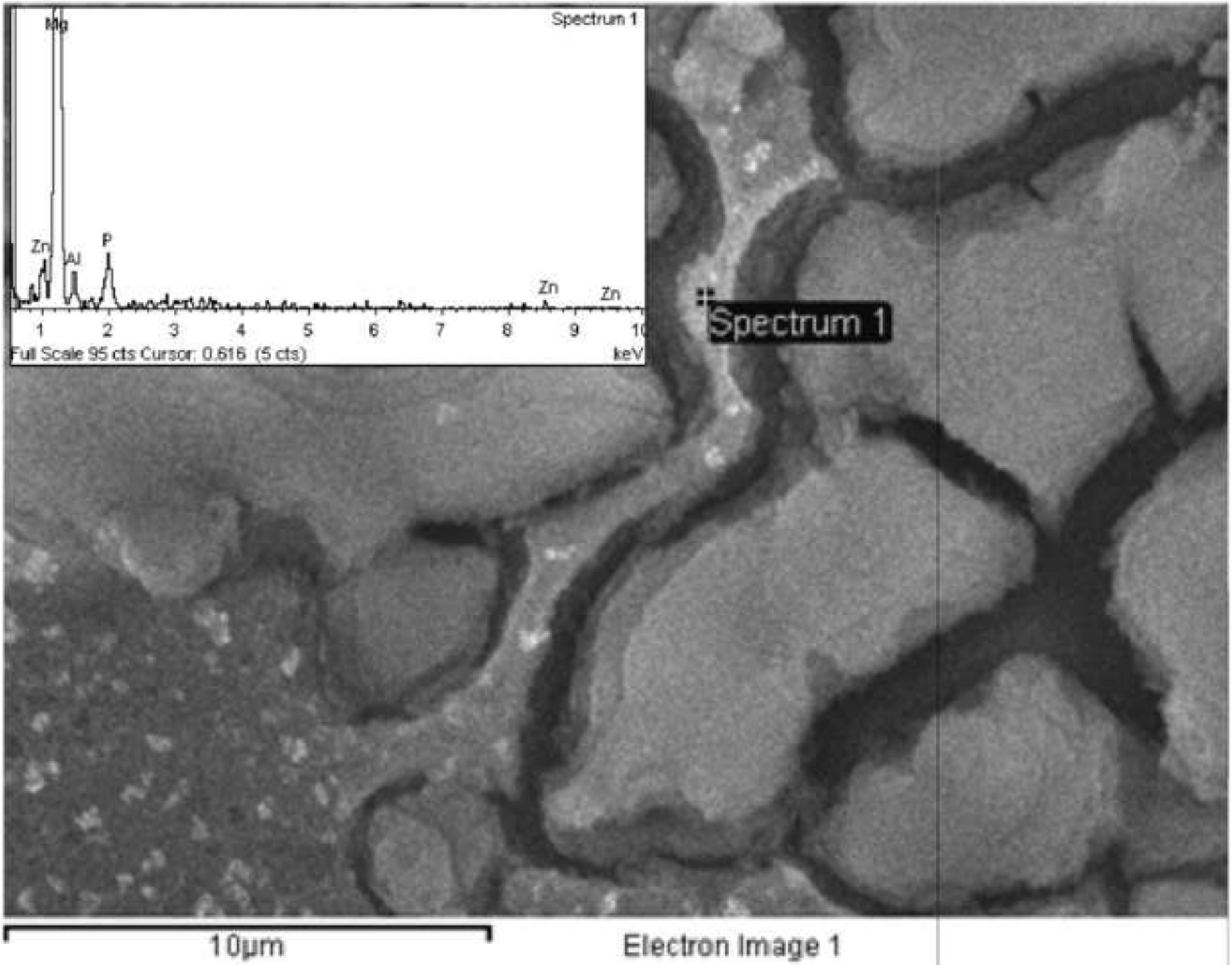

5. Figure(s)9a

Click here to download high resolution image

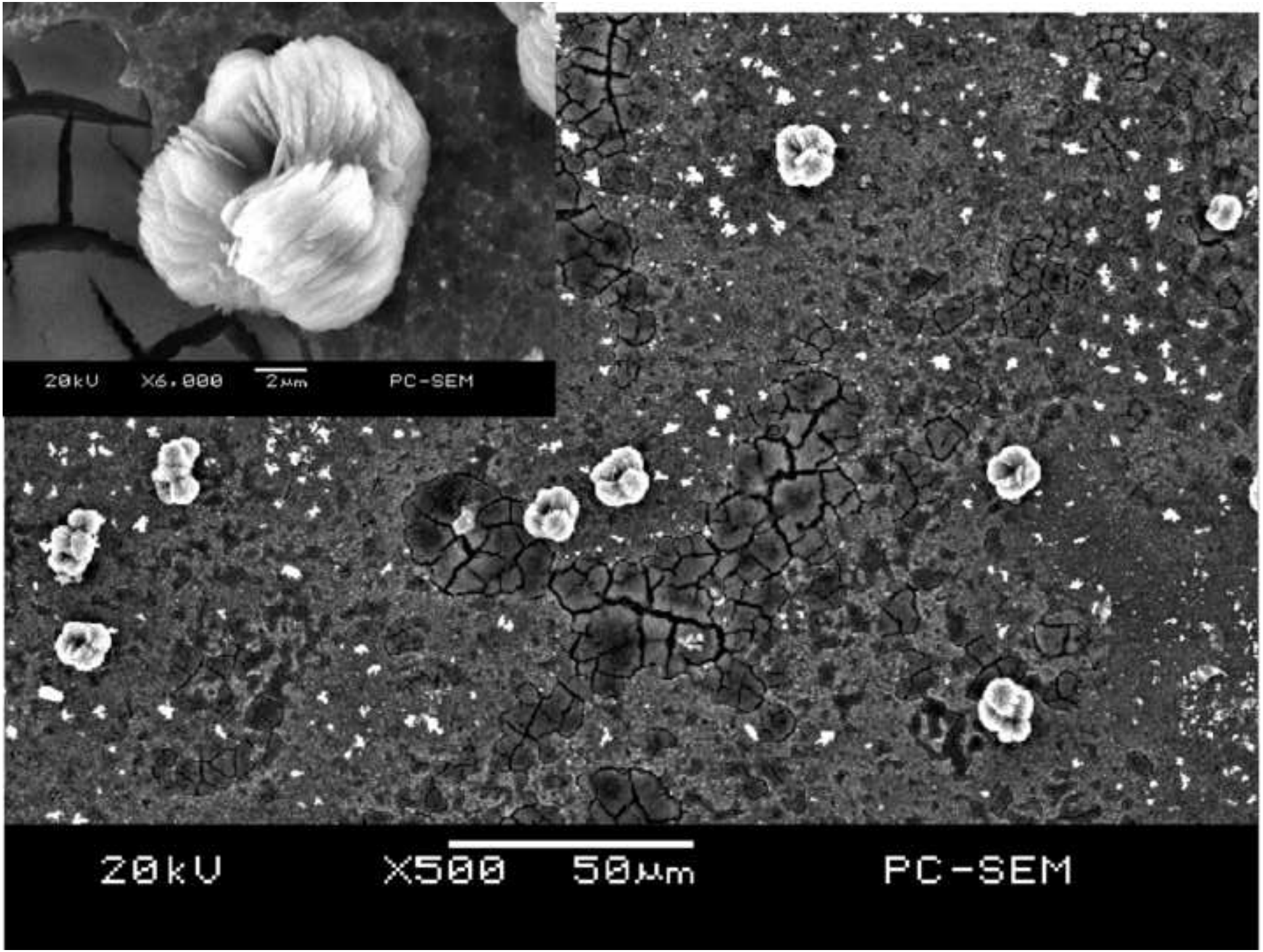

5. Figure(s)9b

Click here to download high resolution image

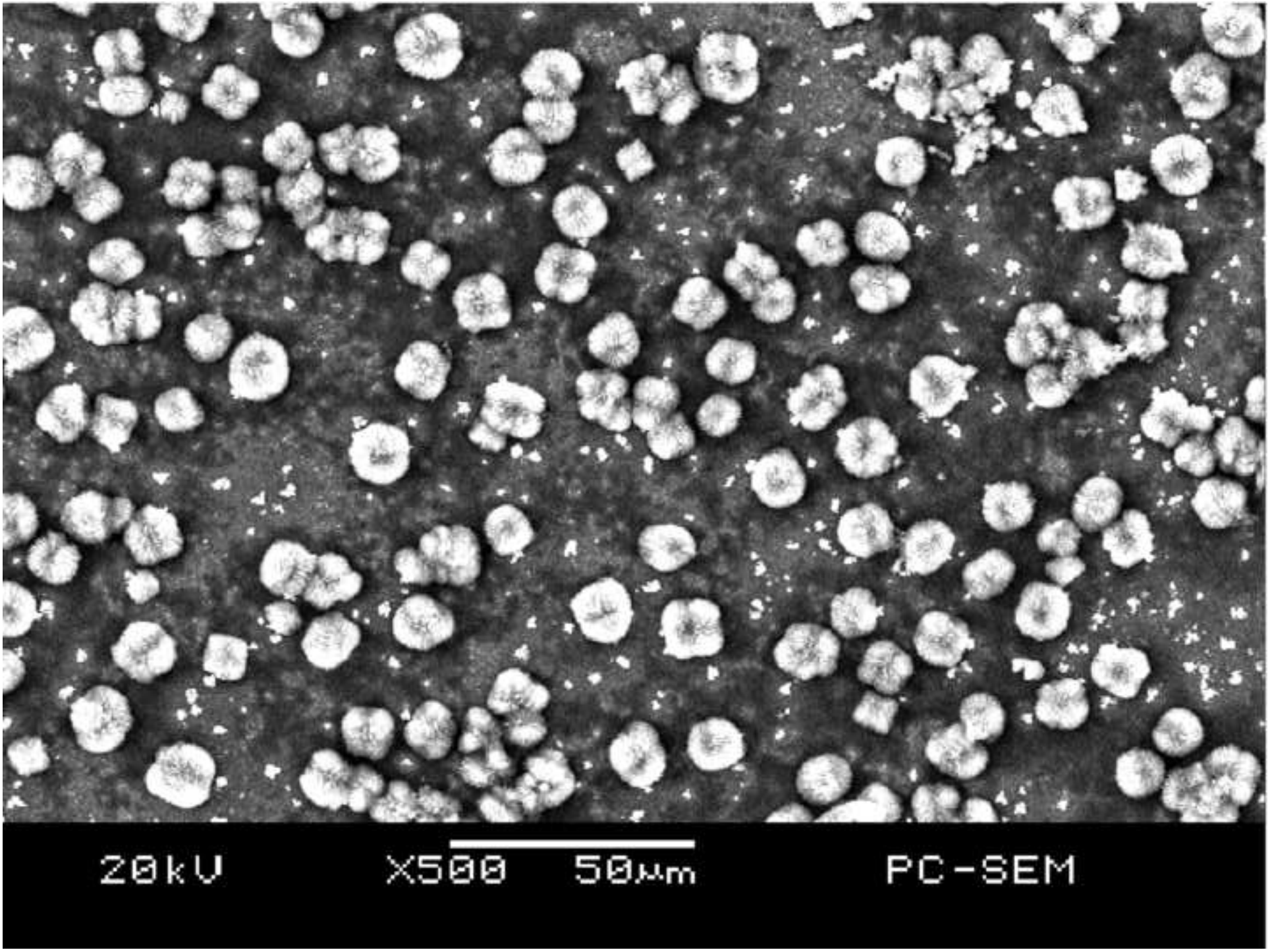

5. Figure(s)9c

Click here to download high resolution image

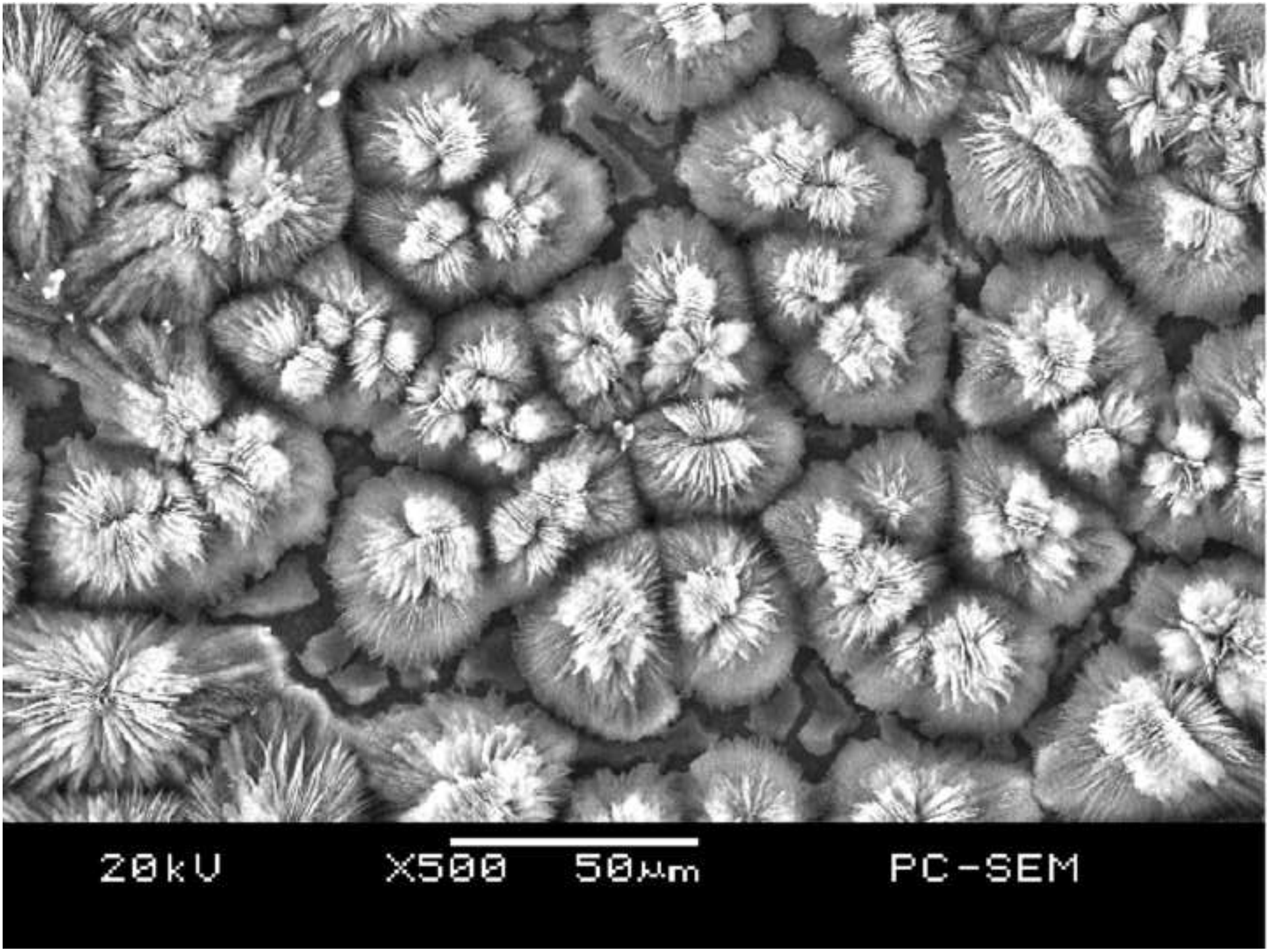

5. Figure(s)9d

Click here to download high resolution image

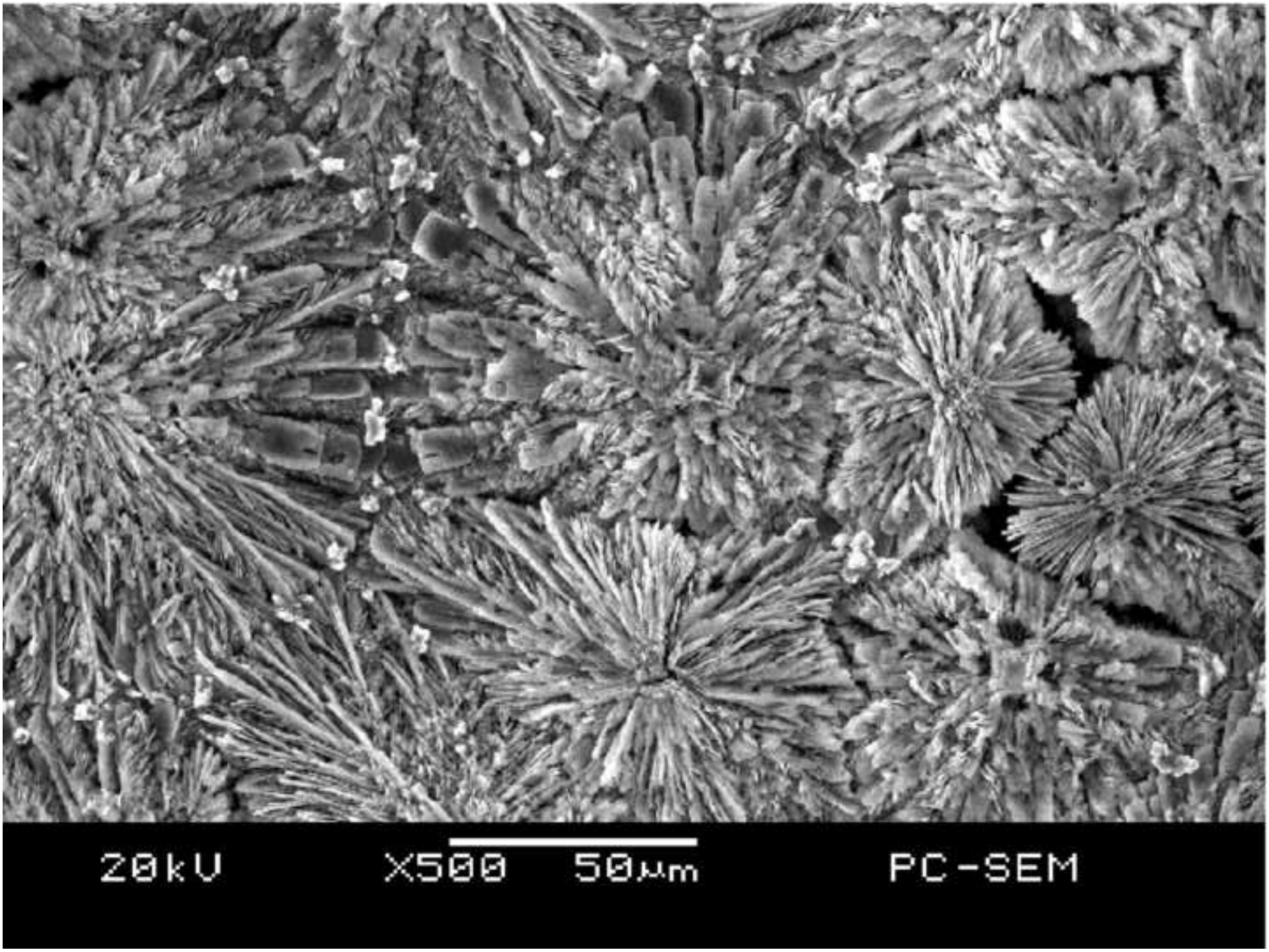

5. Figure(s)9e

Click here to download high resolution image

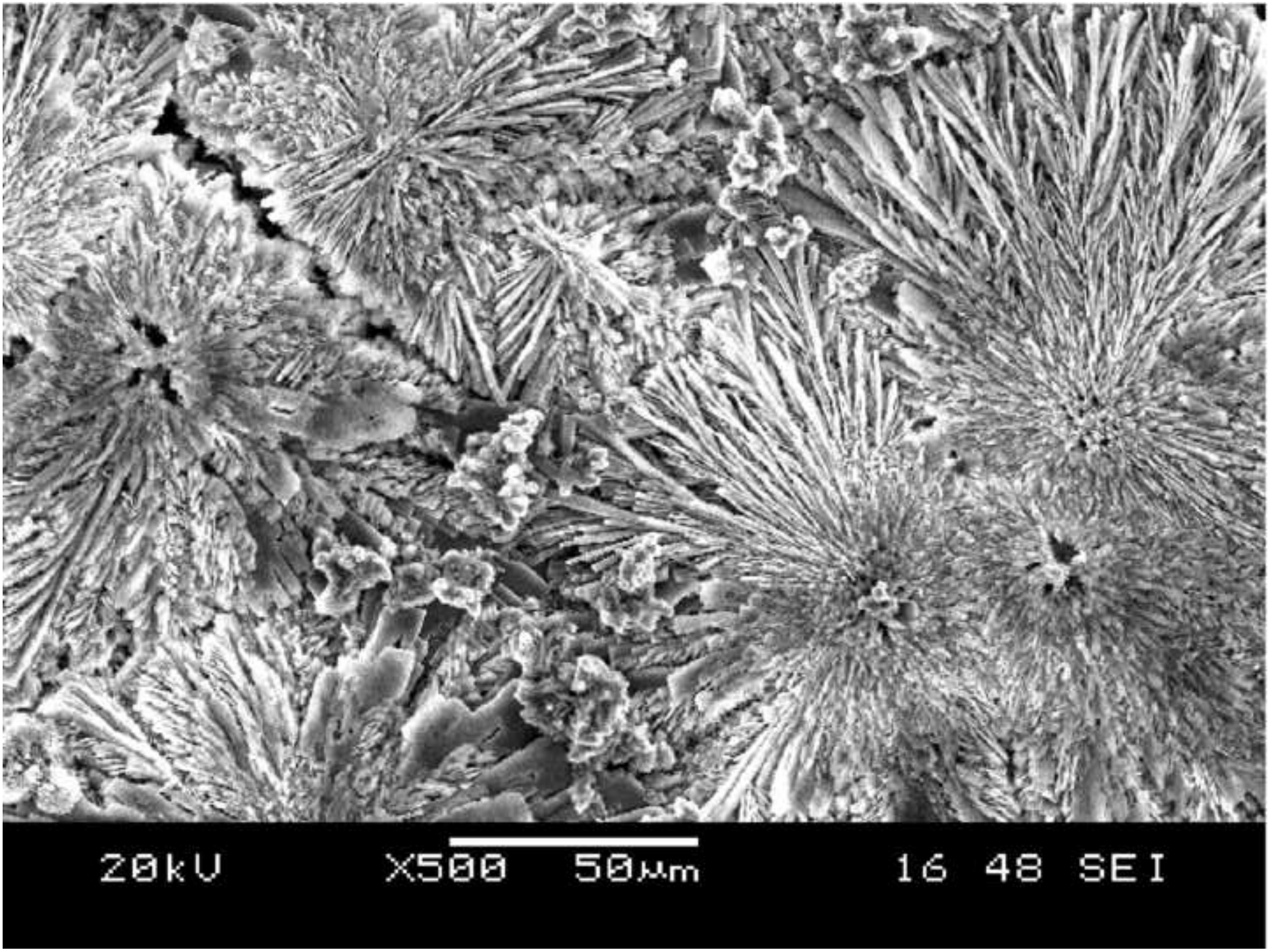

5. Figure(s)9f

Click here to download high resolution image

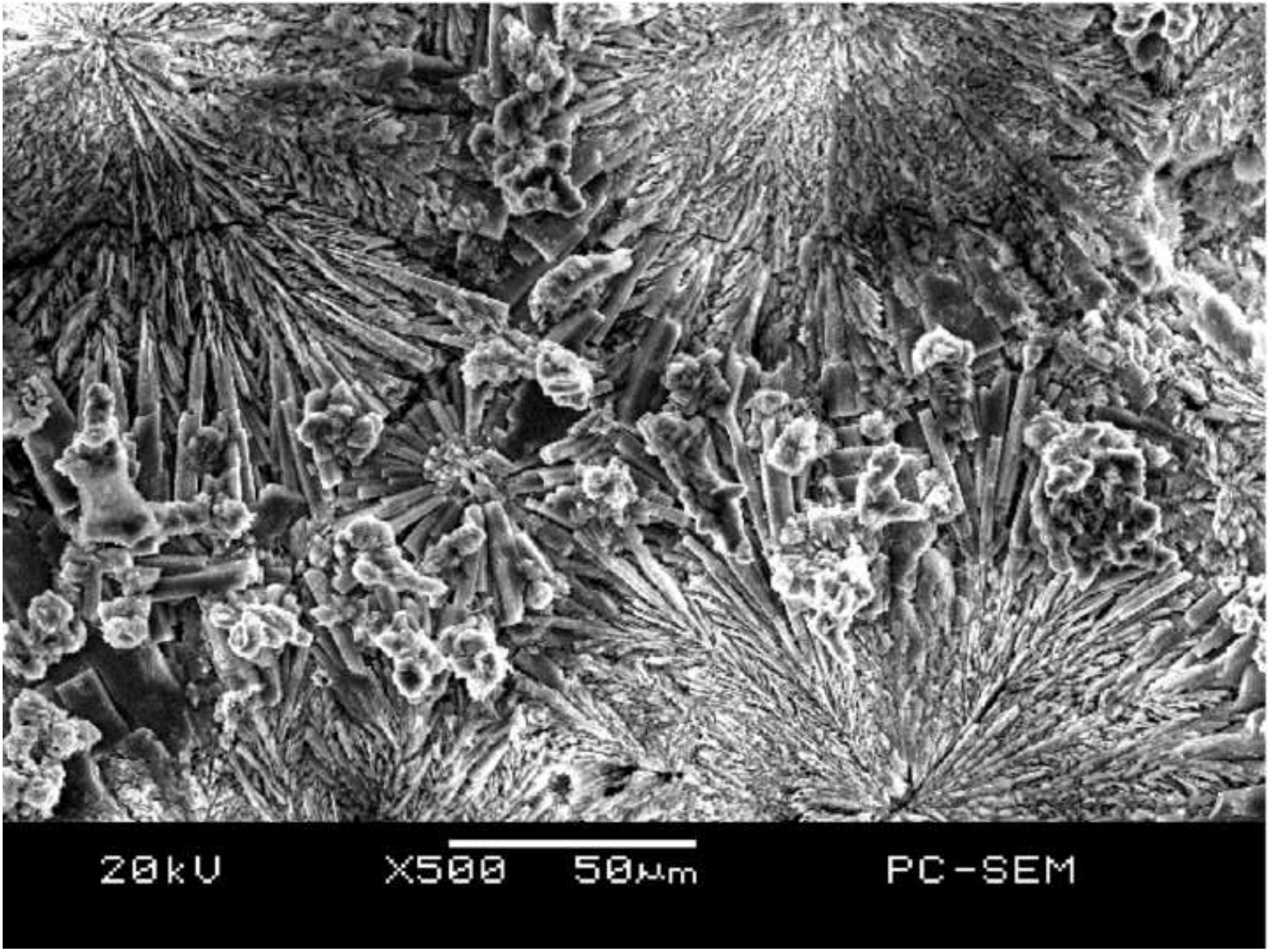

5. Figure(s)10

Click here to download high resolution image